Experimental investigation on the fire resistance of cast-in-situ hollow core concrete slabs constructed using filler boxes and an assembly box system

Ernst & Sohn
A Wiley Brand

Structural Concrete

Experimental investigation on the fire resistance of cast-in-situ hollow core concrete slabs constructed using filler boxes and an assembly box system

Journal:	*Structural Concrete*
Manuscript ID	suco.201800060.R1
Wiley - Manuscript type:	Technical Paper
Date Submitted by the Author:	n/a
Complete List of Authors:	lyu, junli; Shandong Jianzhu University, school of civil engineering wang, yong; China University of Mining & Technology, School of Mechanics & Civil Engineering; China University of Mining & Technology, n/a Van Coile, Ruben; Ghent University, Department of Structural Engineering Huang, Zhaohui; Brunel University College of Engineering Design and Physical Sciences, Department of Mechanical, Aerospace and Civil Engineering Huang, Yuner; The University of Edinburgh, School of Engineering
Subject codes:	testing | experiments, reinforcement, fire protection, design and construction, building materials | construction materials
Keywords:	hollow concrete slab, plastic filler, fire test, temperature, deflection
Abstract:	This paper presents the results of four fire tests on full-scale cast-in-situ, hollow core concrete slabs, constructed using filler boxes and an assembly box system. Experimental data include the furnace temperature, temperature distribution in the slab, and vertical and horizontal deflections during the heating and cooling phases, as well as observed cracking patterns. The test data indicate that the tested hollow slabs with plastic filler boxes have good performance in case of standard fire exposure with small vertical deflections and high deflection recovery in long duration testing. For slabs with assembly box systems serious spalling was observed, resulting in integrity failure after 69 minutes in one of the tests. Nevertheless, load bearing capacity was maintained for all tests. The tests highlight the importance of the boundary conditions and the arrangement of the filler system on the fire behaviour of the hollow slabs, particularly with respect to the observed cracking, spalling and structural integrity.

Experimental investigation on the fire resistance of cast-in-situ hollow core concrete slabs constructed using filler boxes and an assembly box system

(Running head: fire tests of hollow core concrete slabs)

Junli Lyu [a], Yong Wang [b*], Ruben Van Coile [c], Zhaohui Huang [d] , Yuner Huang [e]

[a] School of Civil Engineering, Shandong Jianzhu University, Jinan, China

[b] State Key Laboratory for Geomechanics & Deep Underground Engineering, School of Mechanics & Civil Engineering, China University of Mining & Technology, Xuzhou, Jiangsu 221116, China

[c] Department of Structural Engineering, Ghent University, Belgium

[d] Department of Mechanical, Aerospace and Civil Engineering, Brunel University, UK

[e] School of Engineering, The University of Edinburgh, Edinburgh, Scotland, UK

Abstract: This paper presents the results of four fire tests on full-scale cast-in-situ, hollow core concrete slabs, constructed using filler boxes and an assembly box system. Experimental data include the furnace temperature, temperature distribution in the slab, and vertical and horizontal deflections during the heating and cooling phases, as well as observed cracking patterns. The test data indicate that the tested hollow slabs with plastic filler boxes have good performance in case of standard fire exposure with small vertical deflections and high deflection recovery in long duration testing. For slabs with assembly box systems serious spalling was observed, resulting in integrity failure after 69 minutes in one of the tests. Nevertheless, load bearing capacity was maintained for all tests. The tests highlight the importance of the boundary conditions and the arrangement of the filler system on the fire behaviour of the hollow slabs, particularly with respect to the observed cracking, spalling and structural integrity.

Keywords: hollow concrete slab; plastic filler; fire test; temperature; deflection

[b,*] Corresponding author.

E-mail address: yongwang@cumt.edu.cn

1. Introduction

In recent years, a number of experimental studies have been conducted to investigate the fire behaviour of reinforced concrete slabs (Bailey and Toh, 2007; Li et al., 2015; Lim and Wade, 2002; Wang et al., 2016; Wang et al., 2018; Wang and Dong, 2009; Yang et al., 2013; Zhu, 2012), and it is acknowledged that reinforced concrete floor slabs play a key role in enhancing the fire resistance of the building. However, as noted in the following literature review, most of the tests considered conventional concrete slabs.

Bailey and Toh (Bailey and Toh, 2007) and Lim and Wade (Lim and Wade, 2002) conducted fire tests on simply supported concrete slabs. Wang and Dong (Wang and Dong, 2009) conducted two fire tests on full-scale concrete slabs which were supported on four-edges, considering both simply supported conditions and fixed supports. Zhu (Zhu, 2012) conducted six fire tests of full-scale two-way RC slabs, which included slabs with two edges being clamped, slabs with two edges being simply supported, two-way RC slabs, and flat-plate floors slabs. Wang et al. (Wang et al., 2016 and Wang et al., 2018) conducted nine large scale fire tests on the reinforced concrete slabs under axial in-plane and out-of-plane loading conditions with vertical restraint at four corners of the slabs. In addition, a series of fire tests on a full-scale eight-story steel-framed building were conducted in 1996 (Bailey, 1998; Huang et al., 2003a, 2003b). Recently, several series of full-scale fire tests were conducted on the conventional concrete floor in a full-scale three-story steel-framed building in China (Li et al., 2015; Yang et al., 2013; Wang et al., 2013). These fire tests showed that the deformation process and cracking patterns of the concrete slabs were highly dependent on the restraint conditions, and they exhibited excellent fire resistance performance due to tensile membrane action.

In fact, apart from the conventional solid concrete slabs, hollow core slabs are being increasingly used in building applications. On one hand, many experimental studies have been carried out to evaluate fire resistance of conventional PC hollow slabs (Acker, 2003; Bailey and Lennon, 2008; Chang et al., 2008; Kodur and Shakya, 2017; Lennon, 2003; Shakya and Kodur, 2014). Based on data from these standard fire tests, prescriptive rules have been developed. Thus, the fire resistance of hollow slabs in design is commonly determined based on slab thickness and concrete cover thickness. These prescriptive rules, however, consider only limited parameters and often, do not yield realistic fire resistance. On the other hand, there are other types of concrete hollow slabs which are not explicitly

considered in the prescriptive design rules, such as the cast-in-situ (plastic filler boxes) hollow concrete slabs and assembly box concrete slabs (Zhao et al., 2011). These hollow concrete slabs, which are made of embedded filler boxes, have been widely used in practical projects, because of their large span, short construction period and economic advantages. However, the research on the fire resistance of plastic filler box and assembly box concrete hollow slabs is still limited. Note that, different from that of the assembly box, the plastic box has several shortcomings, including vulnerability, easy damage and inflammability. In addition, the anti-floating method should be used in the construction.

Considering this lack of experimental data, fire tests are conducted on four full-scale cast-in-situ concrete hollow slabs supported by different boundary conditions (simply-supported and column-supported), considering both exposed and concealed boxes. The main objectives of this research are:

- Assess the standard fire performance of the tested slabs (i.e. fire rating classification) and observe failure modes.
- Compare the fire behavior of these hollow slabs with those of conventional concrete slabs.
- Obtain test results on thermal and structural behavior of hollow concrete slabs, to be used for the development of numerical models.

2. Test programme

2.1 Test furnace

As shown in Fig. 1, a modified furnace (6560 mm × 4830 mm × 1500 mm) was specially designed to heat the hollow slabs. A viewing port was placed in the west furnace wall. Note that, according to the dimensions of each specimen, the dimensions of the furnace can be adjusted before each test.

2.2 Test specimens

2.2.1 Cast-in-situ concrete hollow slabs with plastic box fillers

For Test 1, the simply-supported slab was 6680 mm × 4640 mm × 300 mm, as shown in Fig. 2 (a). The slab consist of ribbed beams and 96 plastic boxes creating voids (each plastic box: 450 mm × 450 mm × 150 mm), as shown in Figs. 2(b)-2(f). The plastic box fillers were

grouped per 4 (4 boxes constituting a single filler element), and thus the slab had 24 filler elements. The arrangement of the filler elements is indicated in Figs. 2(a) and 2(f). The cross-section of the hollow slab is shown in Fig. 2(g). The concrete depth above the box filler was 80 mm, and the concrete depth under the filler boxes was 70 mm. The cross-section of edge and ribbed beams are shown in Figs. 2(e) and 2(h).

The tested concrete compressive strength was 33.5 MPa. The slabs were reinforced with hot-rolled reinforcing bars of 8 mm diameter, and the actual yield and ultimate tensile strengths were 538.8 MPa and 640.0 MPa, respectively. Bottom and top reinforcing bars were arranged at a spacing of 200 mm along both directions, as indicated in Figs. 2(e) and 2(f). Similarly, for the ribbed and edge beams, the actual yield and ultimate tensile strength of reinforcement (16 mm) are 466.2 MPa and 628.1 MPa, respectively. The clear concrete cover is 20 mm for all reinforcement. The details of reinforcement arrangement and the plastic boxes in the slab are shown in Figs. 2(a), 2(e) and 2(f).

For Test 2, the column-supported slab was 4560 mm × 4560 mm × 300 mm, as shown in Fig. 3(a). Similarly, it consisted of ribbed beams and 64 plastic box fillers. As four plastic boxes were grouped into a single filler element, the slab has 16 elements. In addition, each concrete column has a square section (300 mm × 300 mm), with the height of 1500 mm. The columns were protected from the fire by mineral wool (its thickness: 50 mm).

The concrete compressive strength was 36.7 MPa at the time of testing. The yield and ultimate tensile strength of the reinforcement (8 mm) were 415 MPa and 510 MPa, respectively. Bottom and top reinforcing bars were arranged at a spacing of 200 mm along both directions, as shown in Fig. 3(b). The edge beams, ribbed beams and columns are shown in Figs. 3(c), 3(d) and 3(e). Similarly, the tested yield and ultimate tensile strength of reinforcement (16 mm) were 407 MPa and 508 MPa, respectively. In addition, the column construction, layout of plastic boxes and casting concrete are shown in Figs. 3(f)-3(h).

2.2.2 Assembly box concrete hollow slabs

As shown in Figs. 4(a) and 4(b), the dimension of the simply supported slab (Test 3) was 6680 mm × 4640 mm × 300 mm, and it consisted of assembly boxes, the ribbed beams and

the edge beams. It is noted that the concrete was not casted on the top surface of the assembly boxes (exposed boxes), and the reinforcing steel was not placed on the top surface of the assembly boxes. The arrangement of the assembly boxes in the slab is indicated in Fig. 4(a).

As shown in Fig. 4(c), one assembly box consisted of one top plate, one rectangular side-wall and one bottom plate. The width and length of one plate was 500 mm × 500 mm with 50 mm of the height. The thickness of the side-wall was 10 mm. Commercial fine aggregate concrete with the compressive strength of 40 MPa was used for the plate. Note that, the commercial fine aggregate concrete was designed according to the reference (JGJ 55-2011, 2011). One plate was reinforced with cold drawn steel of 4 mm diameter (characteristic tensile strength of 550 MPa and spacing of 200 mm).

The cross-section of edge and ribbed beams are shown in Figs. 4(d)-4(g). The beams were reinforced with hot-rolled reinforcing bars of 16 mm diameter (characteristic yield strength of 400 MPa) and the stirrups of 6 mm (characteristic yield strength of 235 MPa). In addition, the concrete cover was 20 mm. The photographs of top (bottom) plate, the side-wall, the assembly boxes and the reinforcing steels are shown in Figs. 4(i)-4(k).

For Test 4, the simply supported slab was 6680 mm × 4800 mm × 350 mm. Similarly, it consisted of 54 assembly boxes, the ribbed beams and edge beams. Note that, different from that of Test 3, concrete (50 mm thickness) was casted on the top surface of the assembly boxes (called concealed boxes), as shown in Figs. 5(a)-5(d). The other details of Test 4 were similar to those of Test 3. The photograph of the assembly boxes and steels in Test 4 are shown in Fig. 5(e).

2.2.3 Concrete

The cast-in-situ concrete that was used in each test was the commercial concrete. The specified compressive strength of the concrete was 30MPa, and concrete mix was shown in Table 1. Slabs in Tests 1 and 2 were cast on the same day and were stored indoors in the laboratory to cure. The same procedure was followed for slabs 3 and 4.

The age of the concrete at the time of testing was: Slab Test 1=150 days; Slab Test 2 =120 days; Slab Test 3=60 days and Slab Test 4=120 days. Due to the testing conditions, the

temperature and relative humidity were not controlled in the laboratory. The average compressive strength of the concrete was determined by three cubic crushing tests at the day of testing, with obtained strength values as discussed above.

2.3 Boundary conditions

Apart from Test 2, the four supported edges of the other three hollow slabs were supported by steel balls and rollers, according to the references (GB/T 9978-2008, 2008; GB/T 50152-2012, 2012). The configuration of steel balls and steel rollers are shown in Fig. 6, and the gap between the slab and the furnace wall was filled with mineral wool.

2.4 Instrumentation

2.4.1 Cast-in-situ concrete hollow slabs

- Test 1

In Test 1, five groups of Type-K thermocouple trees (L1-L5) were used to measure the temperature of the ribbed beams, as shown in Fig. 7(a). Each thermocouple tree consists of 10 thermocouples, as shown in Fig. 7(b). As indicated in Fig. 7(c), five groups of Type-K thermocouple trees (M1-M5) were used to measure the temperature of the hollow slabs. Each thermocouple tree consists of 7 thermocouples, as shown in Fig. 7 (d).

Fig. 7(e) shows the position of vertical and horizontal displacement transducers (with limit travel ranging from 10-500 mm). Seven LVDT's (V1-V7) were placed at the mid-spans and quarter-spans of the slabs to measure vertical deflections, while its horizontal deflections were measured by two LVDT's called H1 and H2, respectively.

- Test 2

For Test 2, the thermocouples were used to measure the concrete temperatures across the thickness of the hollow slab, as shown in Figs. 8(a) and 8(b). The location of the thermocouples is similar to the Test 1 (see Figs. 7(b) and 7(d)). As shown in Fig. 8(c), seven LVDT's were placed at the mid-spans and quarter-spans of the slab to measure vertical deflections. However, the horizontal deflections are not presented in this paper because the transducers were observed to be malfunctioning during the test.

2.4.2 Assembly box concrete hollow slabs

For Tests 3 and 4, as shown in Figs. 9(a) and 9(b), six groups of thermocouple trees (A1-A6)

were used to measure the temperature of the assembly boxes in the test. Each thermocouple tree has three thermocouples.

For Tests 3 and 4, seven groups of thermocouple trees (B1-B7) were used to measure the temperature of the concrete beams, as indicated in Fig. 9(a). Each thermocouple tree consists of 9 thermocouples distributed vertically. For each thermocouple tree in Test 3, seven thermocouples (Points a-g) were used to measure the concrete temperature, two thermocouples (Points h and i) were placed at the mid-height of the top and bottom steel bars, as indicated in Fig. 9(b). Similarly, for each thermocouple tree in Test 4, the thermocouples positions are shown in Fig. 9(c).

As show in Fig. 10, for Tests 3 and 4, five LVDT's (V1-V5) were placed at the mid-spans and quarter-spans of the slab to measure their vertical deflections, while its horizontal deflections were measured by two LVDT's called H1 and H2, respectively.

2.5 Load conditions

For each test, sand bags (each weighing 50 kg) were placed on the slab to simulate the live loads, and the applied loads were equivalent to a uniformly distributed load of 2.0 kN/m^2, which is recommended in the reference (GB/T 50152-2012, 2012).

2.6 Fire type

As discussed above, four fire tests were conducted on an oil-fired furnace, and the fire temperature followed the ISO 834 standard fire curve.

3. Experimental results and discussions

3.1. Test phenomena

3.1.1. Tests 1 and 2

Cracking of the simply supported hollow slab (Test 1) was observed during the test, as shown in Fig.11 (a). As expected, several minutes after ignition, its four corners gradually curled due to the unclamped corners and diagonal cracks could be seen at the corners of the top surface. At approximately 30 min, several cracks (denoted ①, ② and ③) formed on the top surface of the hollow slab. Meanwhile, water and steam started to seep through the cracks. As the test continued, a large amount of water simultaneously seeped through these cracks and accumulated, after which a large amount of steam was driven off. In addition, the crack (denoted ④) across the section of the edge beams gradually appeared in the test. At 1

hour and 50 min, the puddle of water on the top surface of the slab dried up. Finally, the cracking pattern appears on the unheated surface of the slab, as shown in Fig. 11 (a). It can be seen that the central crack (①, ② and ③) tended to be formed across the transverse direction of the slab, this crack pattern was similar to the crack which appears on the conventional simply-supported concrete slabs (Lim and Wade, 2002; Wang and Dong, 2009).

Fig. 11(b) shows the cracking pattern on the top of the column-supported hollow slab. Twenty minutes after ignition, many diagonal cracks (denoted ①) rapidly formed at the corners of the slab adjacent to the columns. Clearly, this behavior is due to the restraint of the column against the curling of the heated slabs. Similarly, water and steam started to seep through the cracks. As the test continues, several major cracks (denoted ②) developed perpendicular to the edge beams. Finally, the crack pattern observed in the slab is shown in Fig. 11(b). Clearly, the cracking pattern in Test 2 was different from that observed in Test 1, and fewer cracks were observed on the central region of the top surface in Test 2. Thus, the comparisons of the cracking patterns for the two slabs indicate that the boundary condition has an important effect on the number and direction of the cracking within the hollow slabs.

Failure mode on the bottom surface of two hollow slabs (Tests 1 and 2) was observed after the test, as shown in Figs. 11 (c) and 11(d). Serious spalling did not occur in the two tests, and thus the two slabs with plastic filler boxes had good fire resistance performance and structural stiffness.

The crack pattern of the two slabs is different from that of the conventional simply-supported and column-supported solid slabs (Lim and Wade, 2002; Wang and Dong, 2009; Zhu, 2002), particularly the crack number and direction. In addition, the failure mode of the present hollow slabs is different from that (shear failure, bond and anchorage failure) of the PC hollow core slabs (Kodur and Shakya, 2014).

As shown in Figs. 11(e) and 11(f), full-depth cracks appeared at the edge beams in Tests 1 and 2. In addition, due to the mineral wool protection, little spalling occurred in the concrete columns (Test 2), as shown in Figs. 11(d), 11(g) and 11(h). However, as shown in Figs. 11(i) and 11(j), the concrete failure of two beam-column connections (i.e., south-east and north-east corners) occurred in Test 2 due to the negative moment, and thus the connections in Test 2 should be reinforced to enhance their fire-resistant performance.

3.1.2. Tests 3 and 4

The following phenomena were observed during the testing of the simply-supported slab in Test 3. Several minutes after ignition, through the viewing ports, the water was seen on the bottom surface of the slab, falling to the ground of the furnace. After that, some noise was heard due to the spalling of the concrete assembly boxes. At approximately 20 min, the bottom failure of several assembly boxes occurred due to the spalling, and thus the bottom reinforcing steel was also observed. It is noted that the very loud noise (spalling) was heard, and the vibration of the slab was observed at the same time. At approximately 25 min, water and steam started to seep through the cracks (on the top surface). Meanwhile, four corners of the slab gradually curled due to the unclamped corners, as shown in Fig. 12 (a). As the test continued, a large amount of water simultaneously seeped through these cracks and accumulated, after which a large amount of steam was driven off, as shown in Fig. 12(b). At that point, the cracking on the unheated surface of the slab could not be observed due to the steam. At 69 min, as shown in Fig. 12(c), one hole was observed on the top surface of the concrete assembly box, and then a flame was observed. Hence, the integrity failure of the slab occurred due to the spalling of the concrete assembly box. At 80 min, three further holes were observed on the top surface of the slab due to the spalling of the assembly boxes (bottom plates), so the hot gases escaped through the holes. At 90 min, the test was stopped in consideration of the safety.

After test, the heated surfaces of the slab were observed, as shown in Fig. 12(d). Clearly, there was serious spalling of the assembly boxes (bottom plates), and several holes at different locations could be seen as well as the bottom reinforcing steels. In other words, the assembly boxes could be resulting in more spalling locally, presumably because they limit the movement of water vapor to the interior of the concrete. In addition, as shown in Fig. 12(e), the steel fracture in the assembly box occurred, and the spalling also appeared on the top plate. However, it is interesting to note that all the ribbed beams did not show the signs of serious spalling.

For Test 4, several minutes after ignition, the noise was heard due to the concrete spalling, and the reinforcing steel could be seen through the viewing port, as shown in Fig. 13(a). It is noted that the concrete spalling, the noise and the vibration lasted until about 40 min. Meanwhile, similar to that of Test 3, water and steam could be seen on the top surface of the slab. At about 40 min, four corners of the slab gradually curled. In addition, the test was stopped from 46 min to 51 min due to the malfunction of the fan. As shown in Fig. 13(b), through the viewing ports, the bottom surfaces of many assembly boxes (bottom plates)

showed signs of serious spalling. At about 70 min, a large amount of water simultaneously seeped through the cracks (top surface) and accumulated, and steam was driven off. Meanwhile, water appeared on the edge beams of the slab, and some inclined cracks (spacing of 300 mm) were observed, as shown in Fig. 13(c). At 292 min, due to the spalling (bottom surfaces) of many assembly concrete boxes, the test was ended. However, different from that of Test 3, no hole was found on the top surface of Test 4 during the heating phase. Hence, the upper cast-in-situ concrete was beneficial to enhance the fire-resistant performance of the hollow slab, particularly the integrity. Similar to that of Test 3, due to the serious spalling, a lot of concrete on the bottom surface had fallen off, and thus the steel bars exposed, as shown in Figs. 13(d) and 13(e). Hence, some methods should be used to reduce the risk of the explosive spalling in the unexposed or exposed assembly boxes. For example, the section shape or section size can be improved and the steel or polypropylene fibers added in the concrete mixes (Majorana et al., 2010). In addition, the slight spalling occurred on the bottom surfaces of the ribbed beams, but no reinforcing steels were observed on the ribbed beams.

3.1.3. Fire resistance

Failure of the slabs is to be evaluated based on different failure criteria discussed in the references (Kodur and Shakya, 2014; Shakya and Kodur, 2015), including integrity, insulation, strength and deflection (ratio) limit state.

The above discussed failure criteria were applied to evaluate fire resistance of the tested slabs, as shown in Table 2. In the present tests, it can be concluded that the strength failure of two slabs (Tests 1 and 4) occurred when considering the simplified criterion of a reinforcement limiting temperature. Nevertheless, each slab sustained service loads for the entire duration of fire exposure, including cooling, and no structural collapse occurred. Thus, the simplified strength failure criterion did not lead to a correct evaluation of fire resistance, since each of the hollow slabs had high structural stiffness and strength at the end of the fire test. However, integrity failure occurred in Test 3, since several holes appeared on the top surface. As Tests 1 and 2 observed limited spalling compared to Tests 3 and 4, it is concluded that the plastic filler systems of the first pair of tests is preferable to the assembly box system of the second test pair. The assembly box system has been observed to result in signification spalling.

3.2. Thermal response

3.2.1 Furnace temperature

The measured average furnace temperatures against time during both the heating and cooling phases for the four tests are shown in Figs. 14 (a)-14(b). The four tests were intended to replicate the ISO834 standard fire curve.

As shown in Figs. 14 (a)-14(b), the fire was characterized by two phases: a growth phase and a decay phase. The shut-off for Tests 1-4 occurred at 212 min, 195 min, 90 min and 292 min after ignition, respectively. Test 3 was stopped early because of an integrity failure of the slab, as discussed. For Tests 1 and 2, their average furnace temperatures are similar to each other. At the shut-off time, the average furnace temperatures recorded in Tests 1-4 were 1115 ^{o}C, 1058 ^{o}C, 824 ^{o}C and 1088 ^{o}C, respectively. After being shut down, the furnace temperature rapidly decreased, and the Tests 1-4 stopped at 600 min, 600 min, 500 min and 1000 min after ignition, respectively.

Note that, for Test 4, due to a short malfunction of the fan, there was a clear decline of the average furnace temperature between 46 min and 51 min. In addition, because of incomplete combustion in the furnace, each average furnace temperature was lower than ISO standard fire.

3.2.2 Temperature of the hollow concrete slabs

(1) Cast-in-situ concrete hollow slabs (Tests 1 and 2)

Figs. 15(a)-15(d) show the temperature profiles at different locations along the cross-sections of two cast-in-situ concrete hollow slabs (Tests 1 and 2). Clearly, the temperature gradients in the two hollow slabs increased quickly with time. For Test 1, at 212 min after ignition, the temperatures at the bottom surface of the slab reached 740 ^{o}C (M2-a) and 757 ^{o}C (M3-a), respectively. Meanwhile, the temperatures at the top surface were 98 ^{o}C (M2-g) and 64 ^{o}C (M3-g), respectively. The difference between bottom and top surfaces at M2 (a-g) and M3 (a-g) were 642 ^{o}C and 693 ^{o}C, respectively. Comparing Figs. 15(a) and 15(b), the overall trend and magnitude of temperatures measured at the two transversal locations are very similar. For Test 2, at 195 min, the temperature differences (Points a and g) were 687 ^{o}C (M1) and 766 ^{o}C (M5), respectively. It is tentatively concluded that the air in the plastic boxes effectively delayed temperature transmission into inner layers. This temperature lag produces high thermal gradients along the depth of the slab during the test.

In addition, for Points M2-d and M3-d (Test 1), there were clear temperature plateaus at about 100 °C attributed to evaporation of moisture. For instance, the plateau duration at Points M8-d and M10-d was 78 min and 162 min, respectively, with the average duration of

120 min. Similar to those of Test 1, there was a pronounced plateau in the temperature rise at Points M1-d and M5-d (Test 2), and the duration of the temperature plateaus was about 130 min (M1-d) and 90 min (M5-d), respectively, and with an average value of 110 min.

As expected, the temperature distribution of the hollow slab is different from those of the conventional concrete slabs (Lim and Wade, 2002; Wang and Dong, 2009; Zhu, 2002) due to the presence of core voids. After the water evaporated, the temperature in the box rapidly increased again. It is noted that the filler reached the highest temperature not at the furnace shut-off time, but at a time behind this. Clearly, this is due to the fact that heat continued to conduct from the heated surface of the hollow slab to the plastic box fillers.

For the unheated surface of the two cast-in-situ hollow slabs, there was a long plateau in the temperature rise at about 100 ^{o}C. The temperature on the unheated surface did not increase during the cooling phase, due to the evaporation of water near to the unexposed surface, the filler acting as a thermal barrier, and thermal inertia of the concrete. According to the conventional temperature failure criterion (ASTM, 2011; BS 476-20, 1987), the hollow slabs have good fire resistant performance, particularly the insulation.

In all, similar to the observation in the reference (Kodur and Shakya, 2017), temperature distribution in hollow core slabs is significantly affected by the presence of hollow cores. The effect of hollow cores on temperature transmission through slab thickness is reflected in temperatures measured within the cores and near to the unexposed surfaces, particularly the temperature plateau. This is mainly due to dissipation of heat (moisture evaporation).

(2) Assembly box concrete hollow slabs

Figs. 15(e)-15(h) show the temperature profiles at different locations in the assembly boxes of the two slabs (Tests 3 and 4). It is noted that the thermocouple of Point A2-1 (Test 3) had a hardware problem at the shut-off time, and the temperature was not recorded during the cooling stage.

On one hand, concrete spalling had an important influence on the temperature distribution of the assembly boxes, particularly the temperature of Point 2. For instance, as shown in Figs. 15(e)-15(g), due to serious concrete spalling of the assembly box slabs, the two thermocouples (Points 1 and 2) were exposed to the fire, and thus the temperatures were similar during the test. In contrast, as shown in Fig. 15(h), in Test 4 the temperatures of Point A2-2 were clearly lower than that of Point A2-1 due to less severe concrete spalling. The observed spalling indicates a need to investigate whether the assembly box system increases

the spalling propensity. An increased tendency to spall could result from the blocking of moisture migration paths by the assembly boxes.

3.2.3 Temperature of the ribbed beams

(1) Concrete temperatures

- Cast-in-situ concrete hollow slabs

Figs. 16(a)-16(d) show the temperature distribution of the ribbed beams in Tests 1 and 2. It can be seen that the temperature developments on each pair of thermocouples were almost the same. Therefore, there is no difference in the temperature distribution along the length of the ribbed beam. The temperatures at all points on the same elevation of a longitudinal section can be considered as homogenous. This is similar to that of the conventional concrete beams (Kodur and Dwaikat, 2007). In Test 1, the temperatures recorded by L1-A and L5-A when the furnace was shut-off, were 721 °C and 650 °C, respectively. Additionally, the similar conclusion can be obtained from Figs. 16(c) and 16(d), and the temperatures recorded by L1-A and L3-A (Test 2) when the furnace was shut-off, were 693 °C and 687 °C, respectively. Meanwhile, a significantly non-uniform temperature distribution is shown in Figs. 16(c) and 16(d) across the cross-section. In Test 2, significant temperature gradients were developed in the bottom part of the ribbed beam at all times of heating. For instance, at the shut-off point, the temperature differences of Trees L1 and L3 were about 600 °C and 613 °C, respectively. Clearly, the temperature distribution of the ribbed beams was similar to that of the slabs' sections (Figs. 15(a)-15(d)).

- Assembly box concrete hollow slabs

Figs. 16(e)-16(h) show the temperature distribution of the ribbed beams in Tests 3 and 4. On one hand, for each slab, the temperature developments of the ribbed beams were similar to each other. On the other hand, the ribbed beams have higher temperature gradients and non-uniform distribution of temperatures over the depth, compared with the temperatures measured at the location of the assembly boxes. For instance, for Test 3, the temperatures recorded by Points B2-a and B7-a when the furnace was shut-off, were 776 °C and 671 °C, respectively. Additionally, the temperatures recorded by Points B2-g and B7-g when the furnace was shut-off, were 23 °C and 50 °C, respectively. The corresponding temperature difference of two measured thermocouple Trees (B2 and B7) were 743 °C and 630 °C, respectively. In addition, for Test 4, the temperature gradient of Trees B1 and B2 were 787 °C

and 760 °C, respectively. It can be seen that the side-walls of the assembly boxes have better heat insulation, and thus the two lateral surfaces of the ribbed beams were not directly heated during the tests. This is different from three heated surfaces (bottom and lateral surfaces) of conventional concrete beams during the fire tests. Hence, compared to the conventional concrete beams, the special construction as part of the hollow slabs leads to their better fire-resistant performance in term of the stability and structural integrity.

(2) Rebar Temperature

- Cast-in-situ concrete hollow slabs

Figs. 17(a) -17(d) illustrate the temperature development of the reinforcing bars in the ribbed beams (Tests 1 and 2). As expected, the temperature curves for the all measured points are similar. However, the temperatures of the bottom reinforcing bars at different positions have a certain difference. For example, as shown in Fig. 17(a), at the shut-off time, the temperatures in the bottom reinforcing bars were 586 °C (L6-J), 624 °C (L1-J) and 426 °C (L2-J), respectively, with the average value of 409 °C. In contrast, it can be seen that the temperature difference of the top steel were relatively lower, as shown in Fig. 17(b). At the shut-off time, the difference between Point L1-K and L3-K were only 38 °C, with an average value of about 79 °C. The similar conclusion can be obtained from Test 2, as shown in Figs. 17(c) and 17(d). At the shut-off time, the average temperature values of bottom and top reinforcing steel bars were 491 °C and 93 °C, respectively.

During the cooling stage, a clear plateau was observed for the temperature at the top reinforcing bars, as shown in Figs. 17(b) and 17(d).

- Assembly box concrete hollow slabs

Figs. 17(e)-17(h) illustrate the reinforcement temperature development of several points in the ribbed beams (Tests 3 and 4). Due to the location of the measured points, the temperatures of the bottom reinforcing bars have a certain difference, as shown in Figs. 17(e) and 17(g). For example, as shown in Fig. 17(e), at 90 min, the temperatures of the bottom reinforcing bars were 220 °C (B1-i), 170 °C (B4-i), 145 °C (B3-i) and 128 °C (B6-i), respectively, with the average value of about 166 °C. Similarly, for Test 4, the bottom steels temperatures at 292 min were 692 °C (B1-i), 625 °C (B4-i), 526 °C (B3-i) and 507 °C (B5-i), respectively, with the average value of about 588 °C. During the cooling stage, for two slabs,

the temperature of the bottom reinforcing bars shortly increased, and then rapidly decreased with the time. At the end of Tests 3 and 4, the average bottom steel temperatures were 94 °C and 140 °C, respectively.

As indicated in Figs. 17(f) and 17(h), for each slab, the temperature difference of the top steels were relatively lower. As expected, there were long temperature plateau at about 100 °C, particularly Test 4 (due to the moisture in the concrete above boxes). At the shut-off time, the average temperatures of top steels (Tests 3 and 4) were 26 °C and 101 °C, respectively. During the cooling stages, similar to the top concrete, the steel temperatures of Tests 3 and 4 gradually increased with time, reaching the maximum values 78 °C and 174 °C, respectively.

Hence, the results indicate that the top steels of the ribbed beams have high strength and fire-resistant performance during the fire tests.

3.3 Deflection response

This section discusses the vertical and horizontal deflections of various structural members during the heating and cooling phases. For the vertical deflection, negative displacement is shown downward; while for the horizontal deflection, negative displacement indicates outward deflection (expansion).

3.3.1 Vertical deflections

- Deflection-time curves

The measured vertical deflections during both the heating and cooling phases for the four hollow slabs are plotted against time, as shown in Figs. 18(a)-18(d). As expected, for Tests 1 to 4, the mid-span deflections were the largest, which reached the maximum values of 73 mm, 92 mm, 35 mm and 77 mm at the corresponding shut-off time, respectively. Clearly, the mid-span deflections of these tests did not reach the normal furnace-test limit of span/30 even when they undergo a long heating period of approximately 5 hours. In contrast, a review of literature shows that the mid-deflections of conventional simply-supported slabs often exceed the limit of span/30 or span/20, if they undergo the similar heating period (Bailey and Toh, 2007; Lim and Wade, 2002; Wang and Dong, 2009; Zhu, 2002; Wang et al, 2016; Wang et al, 2018; Wang et al, 2013; Li et al, 2015). Hence, in term of the structural stiffness and strength, the present tested slabs had good performance compared to what could be expected from the behavior of conventional concrete slabs, although they have higher temperature gradient,

steel temperatures and serious spalling.

Additionally, the relationship between the vertical deflection and time is almost linear, with the deflection rates of 0.34 mm/min, 0.47 mm/min, 0.39 mm/min and 0.26 mm/min, respectively. In other words, these deflections are mainly due to thermal strains generated as a result of high thermal gradients within the cross-section of the slabs. As expected, the deflection trend of the two-way hollow slabs are different from the nonlinear deflection (three-stage mode) observed in one-way PC hollow slabs (Kodur and Shakya, 2014; Kodur and Shakya, 2017; Shakya and Kodur, 2015). On the other hand, the linear trend is different from those observed in the conventional solid slabs. For instance, the tested slabs shows the typical three-stage response mode, in which each stage has unique mechanical characteristics (Wang et al., 2013).

As shown in Figs. 18(a)-18(d), the vertical mid-span deflection of four slabs partially recovered in the cooling stages, and the deflection-time relationship during the cooling phase is nonlinear. On one hand, for Tests 1 and 2, the similar deflection tendency indicates that both hollow slabs exhibited good recovery performance irrespective of different boundary conditions. On the other hand, for Tests 3 and 4, although the serious spalling of the concrete assembly boxes occurred, the spalling of the ribbed beams was relatively slight, and thus the loads during the later stage of fire tests were mainly born by ribbed beams. Hence, it can be seen that due to the presence of the ribbed beams, each hollow slab have high structural stiffness and strength, with different behavior compared to the carrying mechanism (tensile membrane action) of the conventional solid slabs.

- Deflection-average furnace curves

Figs. 19(a)-19(d) show the mid-span deflection against average furnace temperature for the four slabs. Clearly, the mid-span vertical deflection of each hollow slab increased suddenly at about 600 ^{o}C of the furnace temperature. At 600 ^{o}C, the mid-span deflections of four hollow slabs were 12.26 mm, 17.1 mm, 14.4 mm and 21.0 mm, respectively. After that, the mid-span deflection of each slab increased almost linearly the end of the test. This observation is similar to those of the conventional simply-supported slabs (Bailey and Toh, 2007; Lim and Wade, 2002; Wang et al, 2009; Wang et al., 2016; Wang et al., 2018), i.e., when the average furnace temperatures exceed 600 ^{o}C, their mid-span deflection ratio would suddenly increase. This is mainly due to the increasing temperature gradient (thermal bowing) and the decreased material properties.

After the furnace was shut down, the mid-span vertical deflection of each slab gradually recovered. The long plateau in Figs. 19(a)-19(d) corresponds with the fast decrease of furnace temperature after shutdown. Due to the thermal inertia of the slab, the slab deflection does not immediately respond to the reduction in furnace temperature.

3.3.2 Horizontal deflections

Figs. 20(a)-20(c) shows the horizontal deflections of three hollow slabs (Tests 1, 3 and 4) plotted as a function of the time. Due to the devices malfunctioned in Test 2, the horizontal deflection data were lost during the fire test. Clearly, the horizontal deflections of each slab started with outward expansion during the heating stage, followed by contraction during the cooling stage. In the heating phase, the horizontal deflection of each slab gradually increased with increasing fire exposure time. For instance, the maximum horizontal deflections of Tests 1, 3 and 4 were about 10 mm, 4 mm and 55 mm at the shut-off time, respectively.

4 Conclusions

According to test results, the following conclusions can be drawn:

(1) Unlike the conventional concrete slabs, the long temperature plateau (about 100 ^{o}C) was clearly observed near the top surface of each hollow slab. This coincided with large moisture transport and the accumulation of water at the slab top surface. It is suggested that conventional one-dimensional thermal models will need to be expanded to consider moisture transport, and traditional simplified models cannot be used to analyze the temperature distribution of the hollow slab due to its structure.

(2) Each hollow slab has small vertical deflections during the heating stage and deflection recovery during the cooling stage, and thus it has good load carrying capacity irrespective of the serious spalling, larger temperature gradient and long duration of fire. This is considered to be due to the beneficial special structure (ribbed slabs), and the air in the box filler acting as a barrier to heat ingress.

(3) The arrangement of the box fillers have important effects on the failure mode of the hollow slabs, particularly the cracking mode, spalling and integrity.

Acknowledgements

This research was supported by the National Natural Science Foundation of China (Grant No. 51308328 and 51408594), Innovative Research Team in University of Ministry of Education of China (Grant No. IRT13075) and Fundamental Research Funds for the Central

Universities (Grant No.2018QNB10). The authors gratefully acknowledge these supports.

References

Acker V.A. (2003). Shear resistance of prestressed hollowcore floors exposed to fire. *Structural Concrete*, 2003, 4, 65-74.

ASTM (2011). Standard test methods for fire tests of building construction and materials. Test Method E119-12. West Conshohocken (PA): American Society for Testing and Materials.

Bailey C. G. (1998). Computer modelling of the corner compartment fire test on the large-scale Cardington test frame. *Journal of Constructional Steel Research*, 48, 27-45.

Bailey C.G., Lennon T. (2008). Full-scale fire tests on hollowcore floors. *The Structural Engineer*, 86, 33-39.

Bailey C.G., Toh W.S.(2007). Small-scale concrete slab tests at ambient and elevated temperatures. *Engineering Structures*, 29, 2775-2791.

BS 476-20 (1987). Fire tests on building materials and structure-Part 20: Method for determination of the fire resistance of elements of construction. Brussels, Belgium: CEN: European Committee for Standardization.

Chang J.J., Buchanan A.H., Dhakal R.P., Moss P.J.(2008). Hollowcore concrete slab exposed to fire. *Fire and Materials*, 32, 321-331.

GB/T 9978-2008 Fire resistance tests: elements of building (2008). Beijing: Standard Press of China. (in Chinese).

GB/T 50152-2012 Standard for test method of concrete structures (2012). Beijing: China Architecture & Buidling Press. (in Chinese).

Huang Z.H., Burgess I.W., Plank R.J.(2003a). Modeling membrane action of concrete slabs in composite buildings in fire. I: Theoretical development. *Journal of Structural Engineering*, 129, 1093-1102.

Huang Z.H., Burgess I.W., Plank R.J.(2003b). Modeling membrane action of concrete slabs in composite buildings in fire. II: Validations. *Journal of Structural Engineering*, 129, 1103-1112.

JGJ 55-2011 Specification for mix proportion design of ordinary concrete (2011). Beijing: China Architecture & Buidling Press. (in Chinese).

Kodur V.K.R., Dwaikat M.(2007). Performance-based fire safety design of reinforced concrete beams. *Journal of Fire Protection Engineering*, 17, 293-320.

Kodur V.K.R., Shakya A.M.(2017). Factors governing the shear response of prestressed concrete hollowcore slabs under fire conditions. *Fire Safety Journal*, 88, 67-88.

Kodur V.K.R., Shakya A.M.(2014). Modeling the response of precast prestressed concrete hollowcore slabs exposed to fire. *PCI Journal*, 59, 78-94.

Li B., Dong Y.L., Lou Y.J., Wan L.(2015). A fire test of continuous planels in a full-scale steel-frame structure. *Engineer mechanics*, 32, 145-153.(in Chinese).

Lim L., Wade C.(2002). Experimental fire tests of two-way concrete slabs, New Zealand, University of Canterbury.

Lennon T.(2003). Precast concrete hollowcore slabs in fire. *The Structural Engineer*, 81, 30-47.

Majorana C. E., Salomoni V. A., Mazzucco G., Khoury G A. (2010). An approach for modelling concrete spalling in finite strains. *Mathematics and Computers in Simulation*, 80: 1694-1712.

Shakya A.M., Kodur V.K.R.(2015). Response of precast prestressed concrete hollowcore slabs under fire conditions. *Engineering Structures*, 87, 126-138.

Yang Z.N., Dong Y.L., Xu W.J.(2013). Fire tests on two-way concrete slabs in a full-scale multi-storey steel-framed building. *Fire Safety Journal*, 58, 38-48.

Wang Y., Dong Y.L., Zhou G.C.(2013). Nonlinear numerical modeling of two-way reinforced concrete slabs subjected to fire. *Computers and Structures*, 119, 23-36.

Wang Y., Yuan G.L, Huang Z.H, et al (2016). Experimental study on the fire behaviour of reinforced concrete slabs under combined uni-axial in-plane and out-of-plane loads. *Engineering Structures*, 128, 316-332.

Wang Y., Luke A. Bisby, Wang T.Y., et al.(2018). Fire behaviour of reinforced concrete slabs under combined biaxial in-plane and out-of-plane loads. *Fire Safety Journal*, 96, 27-45.

Wang Y., Dong Y.L., Li B., Zhou G.C.(2013). A fire test on continuous reinforced concrete slabs in a full-scale multi-story steel-framed building. *Fire Safety Journal*, 61, 232-242.

Wang B., Dong Y.L.(2009). Experimental research of four-edge simple support two-way reinforced concrete slab under fire. *Journal of Building Structures*, 30, 23-33.(in Chinese).

Zhu C.J.(2012). Studies on fire resistance properties of full-scale two-way reinforced concrete slabs. PhD thesis, Harbin Institute of Techonology, China.(in Chinese).

Zhao K.Z., Li Z.R., Wang L, et al. (2011). Experimental study on mechnical performace of assembly box concrete hollow floor structure with assembly style. *Engineering Mechanics*, 28, 145-150. (in Chinese).

Figures

Fig.1 The testing furnace (all dimensions in mm)

Fig. 2 Details of the various structural elements of Test 1 (all dimensions in mm). (a) Dimensions; (b) Section 1-1; (c) One plastic box (open); (d) One plastic box (closed); (e) Arrangement of reinforcing bars; (f) Layout of plastics boxes (closed); (g) Edge beam; (h) Ribbed beam.

Fig. 3 Details of the various structural elements in Test 2 (all dimensions in mm). (a) Dimensions; (b) Steel bars; (c) Edge beam; (d) Ribbed beam; (e) Column; (f) Column construction; (g) Layout of plastics boxes; (h) Casting concrete.

Fig.4 Details of the various structural elements of Test 3 (all dimensions in mm). (a) Dimensions; (b) Section 1-1; (c) Assembly box; (d) Ribbed beam; (e) Edge beam 1; (f) Edge beam 2; (g) Edge beam 3; (h) Bottom (top) plate of the assembly box; (i) Installation photo for the side wall of the assembly box; (j) An assembly box; (k) Layout of exposed assembly boxes.

Fig. 5 Details of the various beams and assembly boxes of the hollow slab in Test 4 (all dimensions in mm). (a) Ribbed beam; (b) Edge beam 1; (c) Edge beam 2; (d) Edge beam 3; (e) Layout of unexposed assembly boxes and steels.

Fig. 6 .Configuration of steel balls and steel rollers.

Fig. 7 Positions and details of thermocouple trees and displacement transducers in Test 1 (all dimensions in mm). (a) Temperature measurement points of ribbed beams; (b) Thermocouple trees in the ribbed beam; (c) Temperature measurement points of plastic boxes; (d) Thermocouple trees in the plastic box; (e) Positions of the vertical and horizontal displacement transducers.

Fig.8 Typical layout of thermocouples and displacement transducers in Test 2 (all dimensions in mm). (a) Measured points M1~M5; (b) Measured points L1~L5; (c) Displacement transducers.

Fig. 9 Positions and details of thermocouple trees in Tests 3 and 4 (dimensions in mm). (a) Measured points in Tests 3 and 4; (b) Thermocouple trees in Test 3; (c) Thermocouple trees in Test 4.

Fig. 10 Positions of vertical and horizontal displacement transducers in Tests 3 and 4 (dimensions in mm).

Fig. 11 Cracking pattern, spalling and failure of the hollow slabs in Tests 1 and 2. (a) Top surface in Test 1; (b) Top surface in Test 2; (c) Bottom surface in Test 1; (d) Bottom surface in Test 2; (e) Edge beam in Test 1; (f) Edge beam in Test 2; (g) South-east corner column in Test 2; (h) North-east corner column in Test 2; (i) Beam-column connection in Test 2 (South-east corner); (j) Beam-column connection in Test 2 (North-east corner).

Fig. 12 Photographs of the fire test (Test 3). (a) Curled corner; (b) Water on the top surface; (c) One hole on the top surface; (d) Bottom surface after fire test; (e) Steel fracture and spalling of the assembly box.

Fig. 13 Photographs of the fire test (Test 4). (a) Concrete spalling of the bottom plate; (b) Spalling of assembly box; (c) Inclined cracks on the edge beam; (d) Bottom surface of the slab; (e) Spalling on the top plate of the assembly box.

Fig.14 Average furnace temperature versus time in Tests 1-4. (a) Average furnace temperature versus time in Tests 1 and 2; (b) Average furnace temperature versus time of Tests 3 and 4.

Fig. 15 Temperature versus time of the hollow slabs in Tests 1-4. (a) M2 (Test 1); (b) M3 (Test 1); (c) M1 (Test 2); (d) M5 (Test 2); (e) Tree A2 (Test 3); (f) Tree A4 (Test 3); (g) Tree A1 (Test 4); (h) Tree A2 (Test 4).

Fig. 16 Temperature versus time of the ribbed beams in Tests 1-4. (a) L5 (Test 1); (b) L1 (Test 1); (c) L1 (Test 2); (d) L3 (Test 2); (e) Tree B2 (Test 3); (f) Tree B7 (Test 3); (g) Tree B1 (Test 4); (h) Tree B2 (Test 4).

Fig. 17 Temperature of the reinforcing bars in ribbed beams of four tests. (a) Bottom steel bars (Test 1); (b) Top steel bars (Test 1); (c) Bottom steel bars (Test 2); (d) Top steel bars (Test 2); (e) Bottom reinforcing

steels (Test 3); (f) Top reinforcing steels (Test 3); (g) Bottom reinforcing steels (Test 4); (h) Top reinforcing steels (Test 4).

Fig. 18 Vertical displacement versus time in Tests 1-4. (a) Test 1; (b) Test 2; (c) Test 3; (d) Test 4.

Fig. 19 Vertical displacement versus furnace temperature in Tests 1-4; (a) Test 1; (b) Test 2; (c) Test 3; (d) Test 4.

Fig. 20 Horizontal displacement versus time in Tests 1, 3 and 4. (a)Test 1; (b) Test 3; (c) Test 4.

Tables

Table 1 Normal weight concrete mixture design

Normal weight concrete	Mixture ratios			Quantities (kg/m^3)			
	W/*C*	*S*/*C*	*G*/*C*	*W*	*C*	*S*	*G*
	0.53	2.0	2.99	195	368	735	1102

Note: *W*=water; *C* = cement; *S* = sand; and *G* = gravel (calcareous aggregate).

Table 2 Fire resistance measured based on different failure criteria

Test slab	Test duration (min)	Fire resistance (min)				
		Integrity criterion	Insulation criterion	Strength criterion	Deflection criterion	Deflection ratio criterion
Test 1	212	n.f.	n.f.	194	n.f.	n.f.
Test 2	195	n.f.	n.f.	n.f.	n.f.	n.f.
Test 3	90	69	n.f.	n.f.	n.f.	n.f.
Test 4	292	n.f.	n.f.	233	n.f.	n.f.

Note: 'n.f.'=no failure

Fig.1

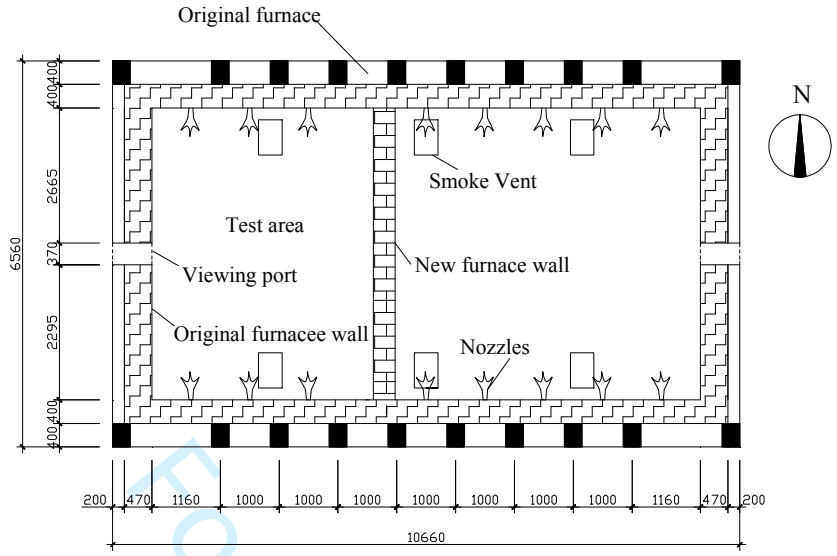

Fig.1 The testing furnace (all dimensions in mm)

Fig.2

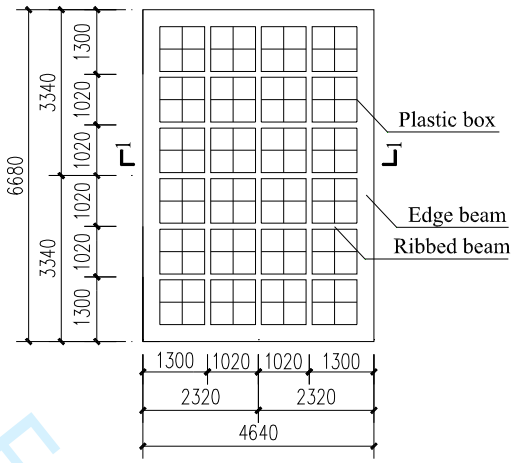

(a) Dimensions

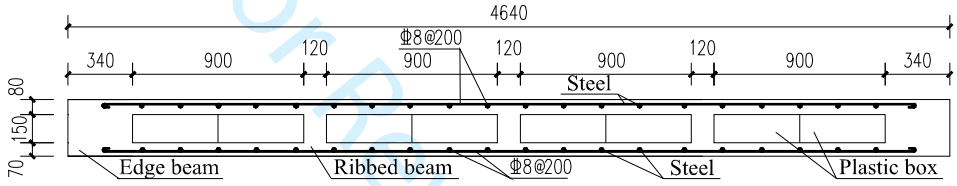

(b) Section 1-1

(c) One plastic box (open)

(d) One plastic box (closed)

(e) Arrangement of reinforcing bars

(f) Layout of plastics boxes (closed)

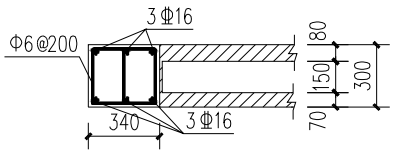

(g) Edge beam

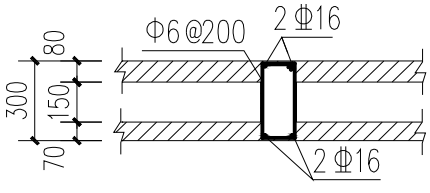

(h) Ribbed beam

Fig. 2 Details of the various structural elements of Test 1 (all dimensions in mm).

Fig.3

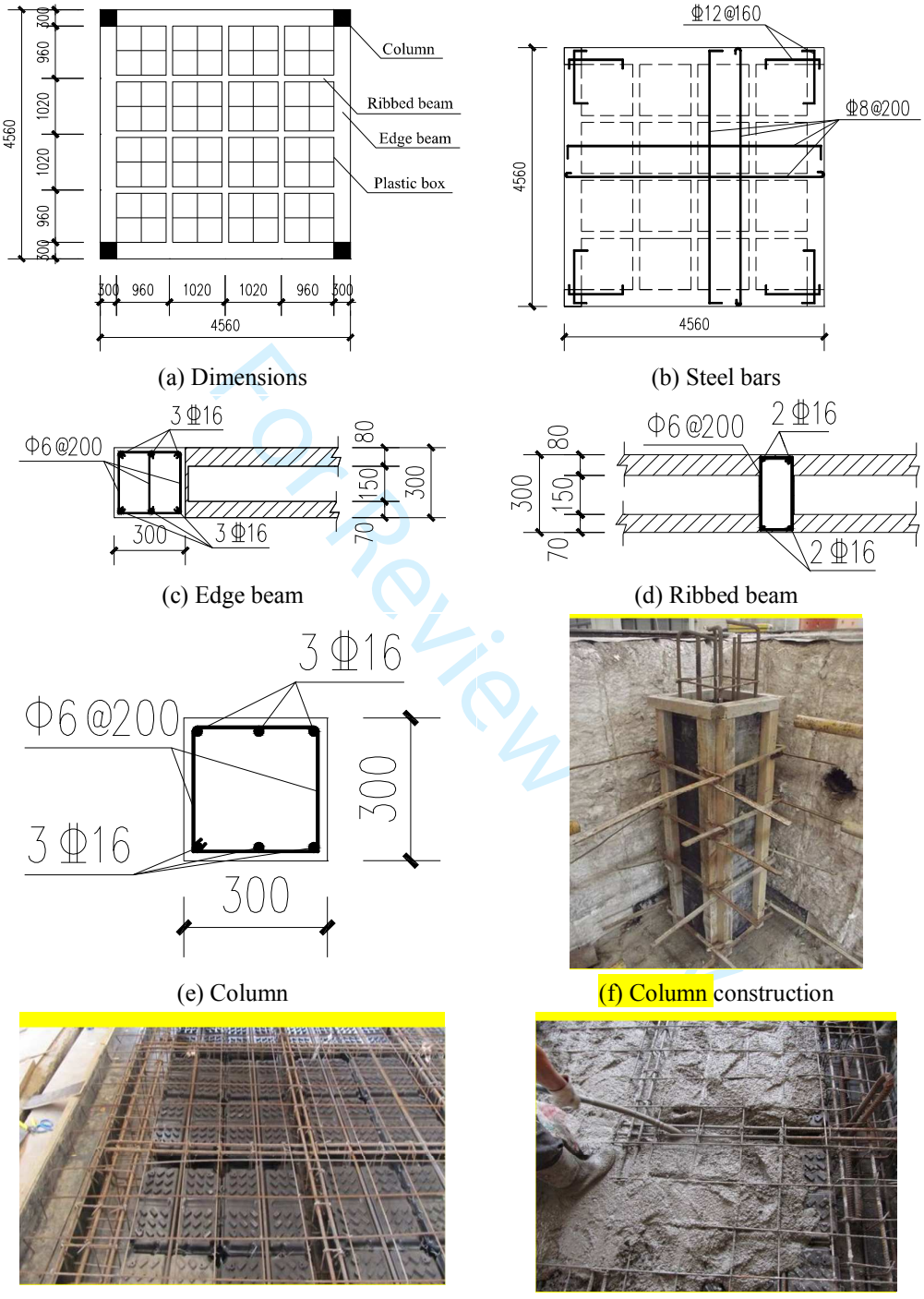

(a) Dimensions (b) Steel bars

(c) Edge beam (d) Ribbed beam

(e) Column (f) Column construction

(g) Layout of plastics boxes (h) Casting concrete

Fig. 3 Details of the various structural elements in Test 2 (all dimensions in mm).

Fig.4

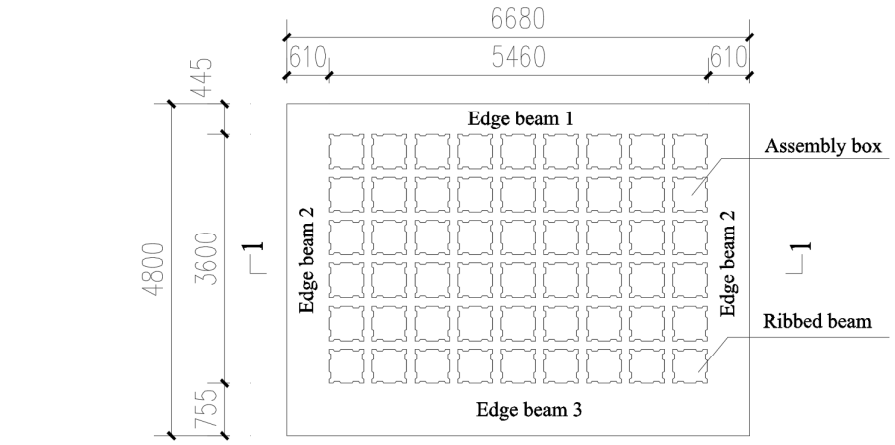

(a) Dimensions

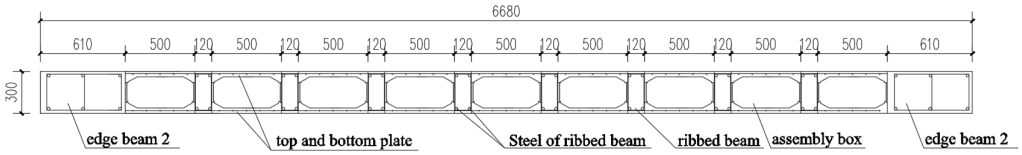

(b) Section 1-1

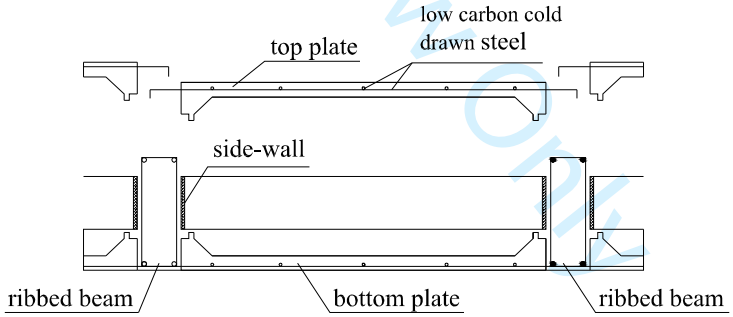

(c) Assembly box

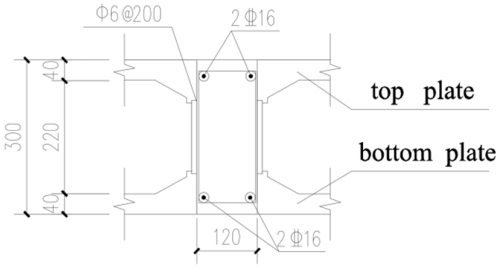

(d) Ribbed beam

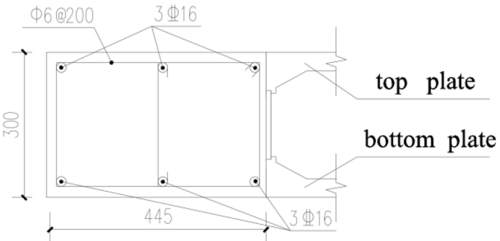

(e) Edge beam 1

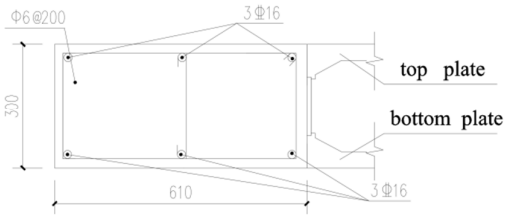

(f) Edge beam 2

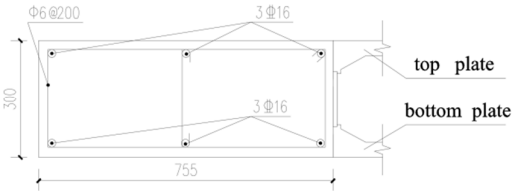

(g) Edge beam 3

(h) Bottom (top) plate of the assembly box

(i) Installation photo for the side wall of the assembly box

(j) An assembly box

(k) Layout of exposed assembly boxes

Fig.4 Details of the various structural elements of Test 3 (all dimensions in mm)

Fig.5

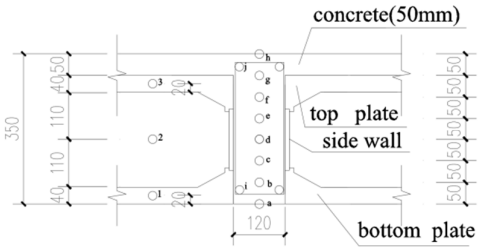

(a) Ribbed beam

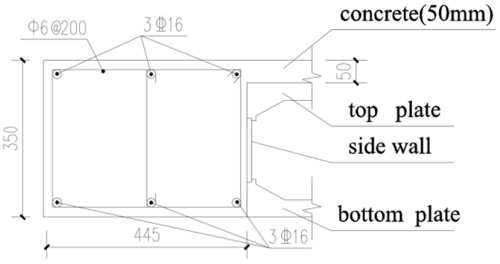

(b) Edge beam 1

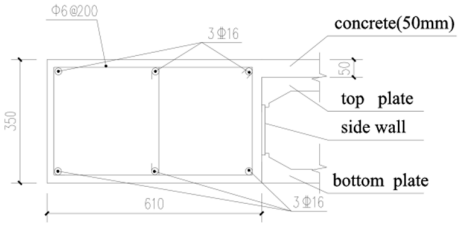

(c) Edge beam 2

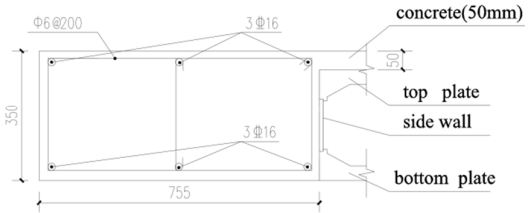

(d) Edge beam 3

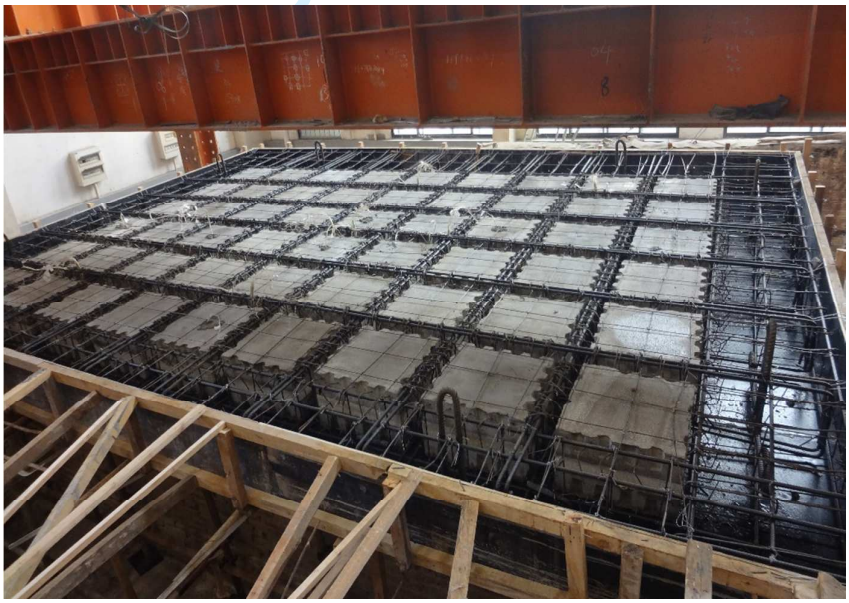

(e) Layout of unexposed assembly boxes and steels

Fig. 5 Details of the various beams and assembly boxes of the hollow slab in Test 4 (all dimensions in mm).

Fig.6

Fig. 6 .Configuration of steel balls and steel rollers

Fig.7

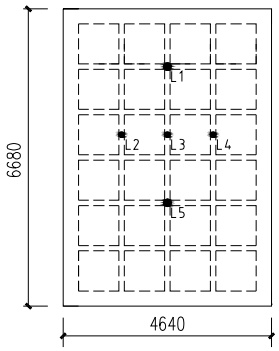

(a) Temperature measurement points of ribbed beams

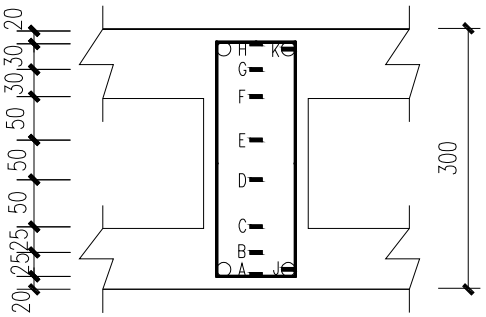

(b) Thermocouple trees in the ribbed beam

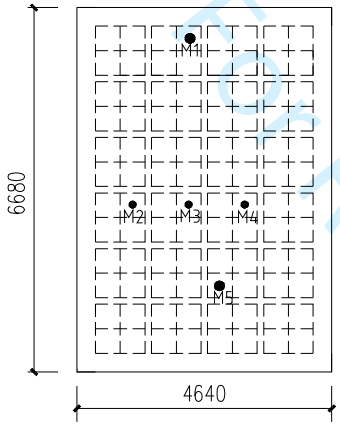

(c) Temperature measurement points of plastic boxes

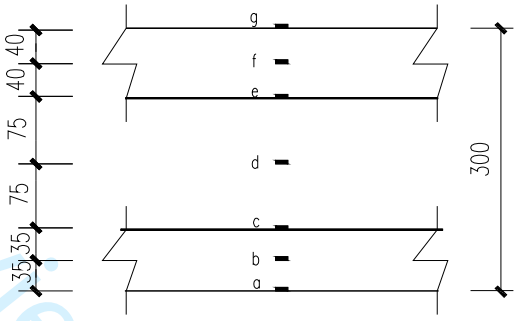

(d) Thermocouple trees in the plastic box

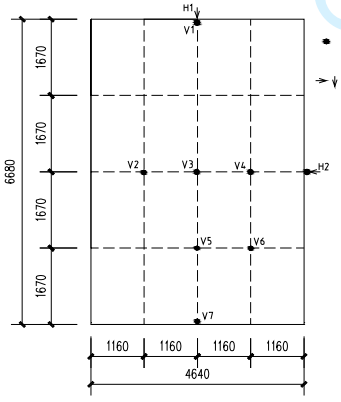

(e) Positions of the vertical and horizontal displacement transducers

Fig. 7 Positions and details of thermocouple trees and displacement transducers in Test 1 (all dimensions in mm)

Fig.8

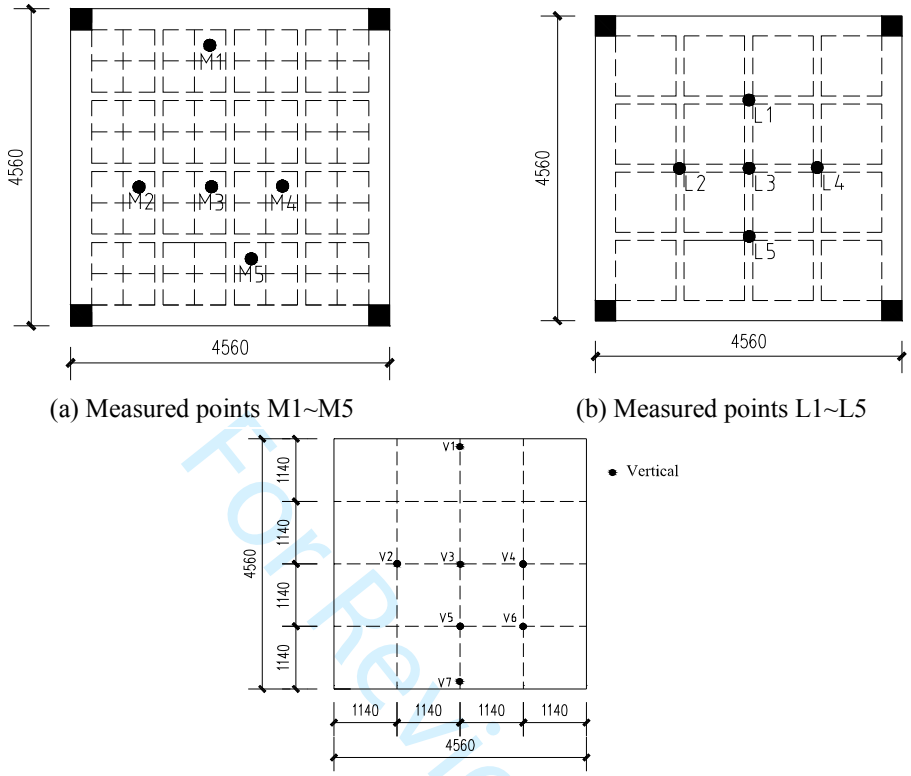

(a) Measured points M1~M5 (b) Measured points L1~L5

(c) Displacement transducers

Fig.8 Typical layout of thermocouples and displacement transducers in Test 2
(all dimensions in mm)

Fig.9

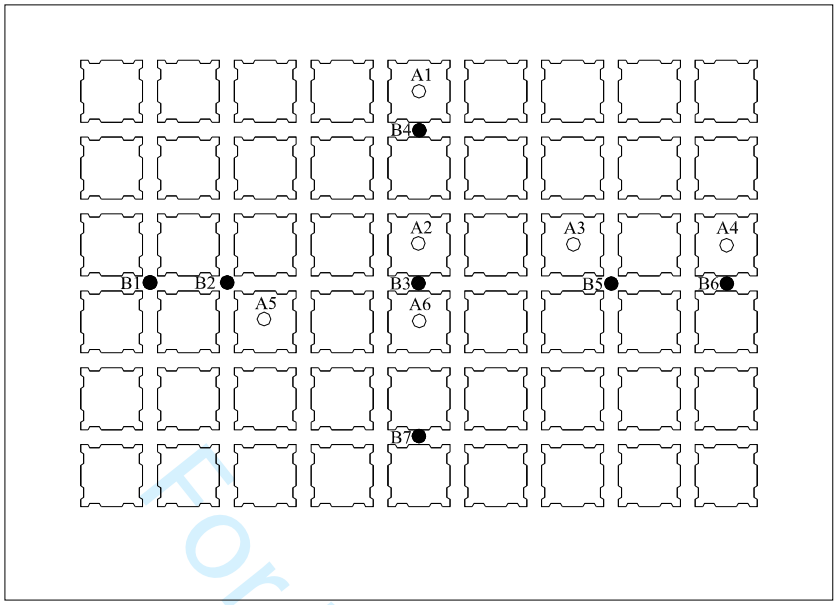

(a) Measured points in Tests 3 and 4

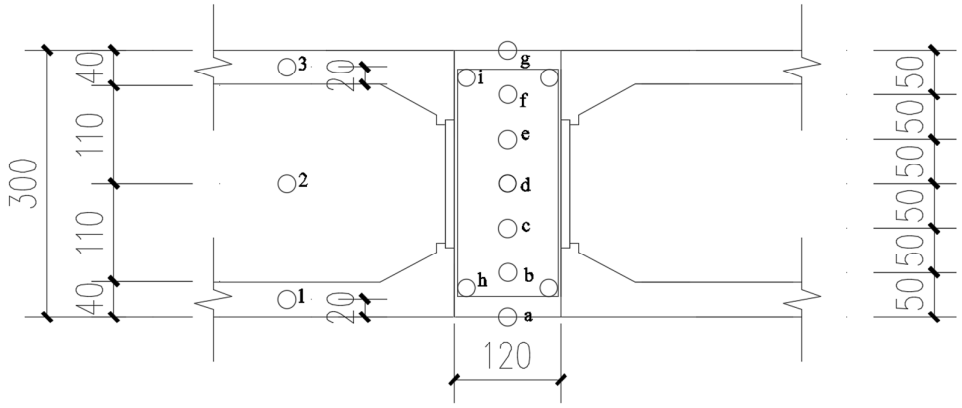

(b) Thermocouple trees in Test 3

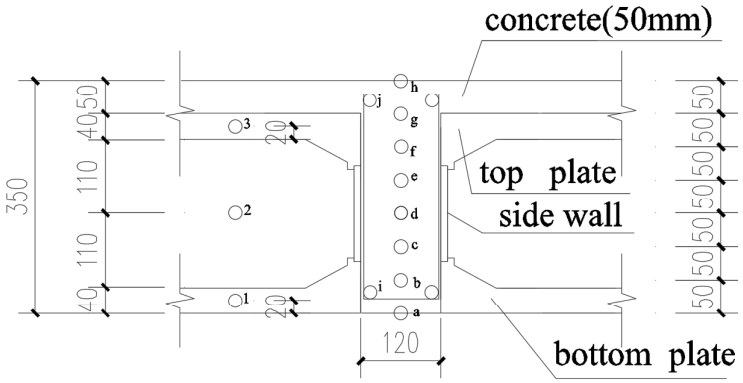

(c) Thermocouple trees in Test 4

Fig. 9 Positions and details of thermocouple trees in Tests 3 and 4 (dimensions in mm)

Fig.10

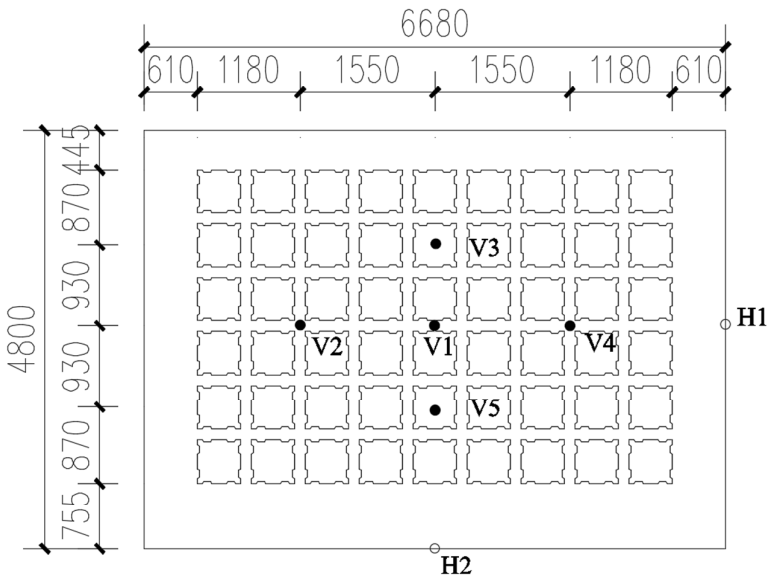

Fig. 10 Positions of vertical and horizontal displacement transducers in Tests 3 and 4 (dimensions in mm)

Fig.11

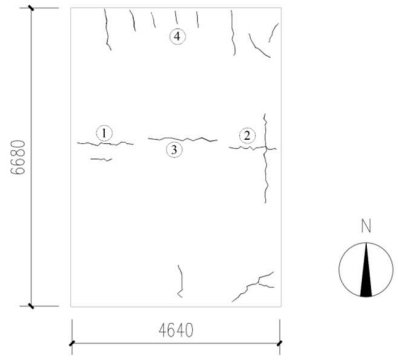

(a) Top surface in Test 1

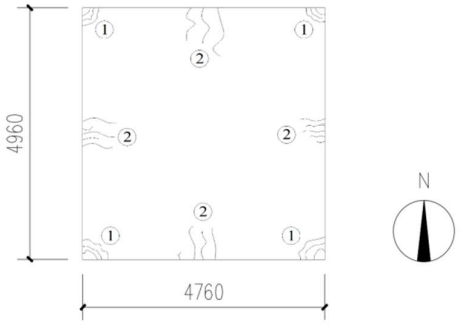

(b) Top surface in Test 2

(c) Bottom surface in Test 1

(d) Bottom surface in Test 2

(e) Edge beam in Test 1

(f) Edge beam in Test 2

(g) South-east corner column in Test 2

(h) North-east corner column in Test 2

(i) Beam-column connection in Test 2 (South-east corner)

(j) Beam-column connection in Test 2 (North-east corner)

Fig. 11 Cracking pattern, spalling and failure of the hollow slabs in Tests 1 and 2

Fig.12

(a) Curled corner

(b) Water on the top surface

(c) One hole on the top surface

(d) Bottom surface after fire test

(e) Steel fracture and spalling of the assembly box

Fig. 12 Photographs of the fire test (Test 3)

Fig.13

(a) Concrete spalling of the bottom plate

(b) Spalling of assembly box

(c) Inclined cracks on the edge beam

(d) Bottom surface of the slab

(e) Spalling on the top plate of the assembly box

Fig. 13 Photographs of the fire test (Test 4)

Fig.14

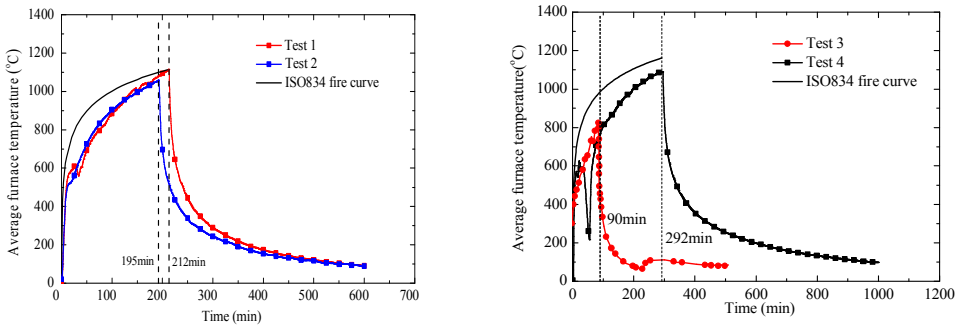

(a) Average furnace temperature versus time in Tests 1 and 2

(b) Average furnace temperature versus time of Tests 3 and 4

Fig.14 Average furnace temperature versus time in Tests 1-4

Fig.15

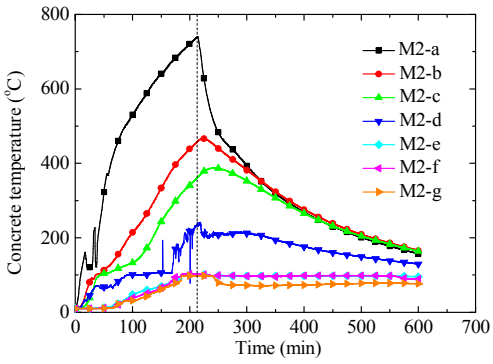

(a) M2 (Test 1)

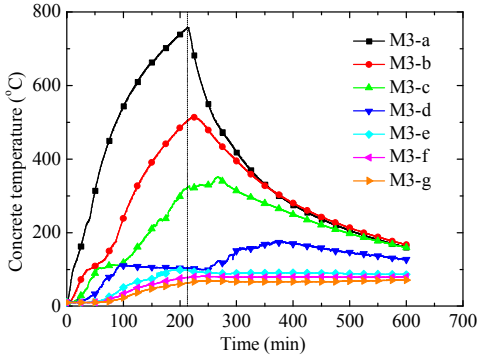

(b) M3 (Test 1)

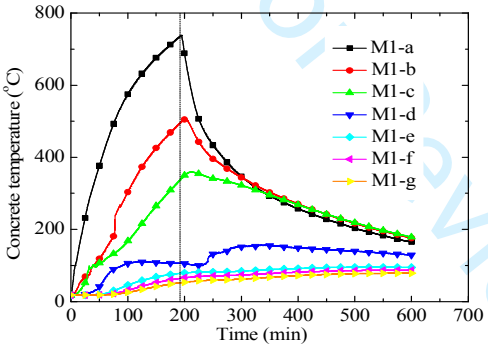

(c) M1 (Test 2)

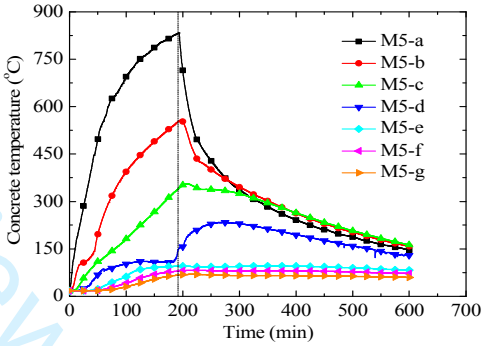

(d) M5 (Test 2)

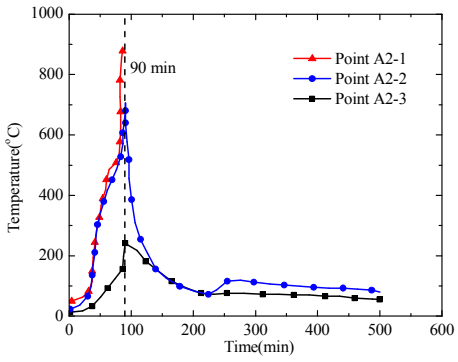

(e) Tree A2 (Test 3)

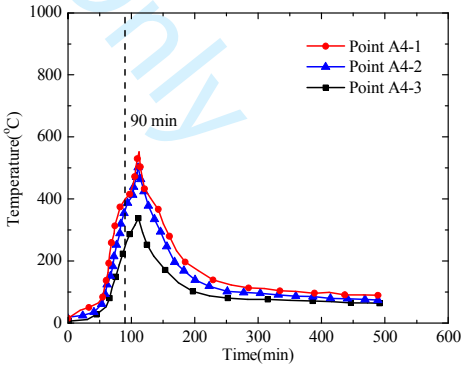

(f) Tree A4 (Test 3)

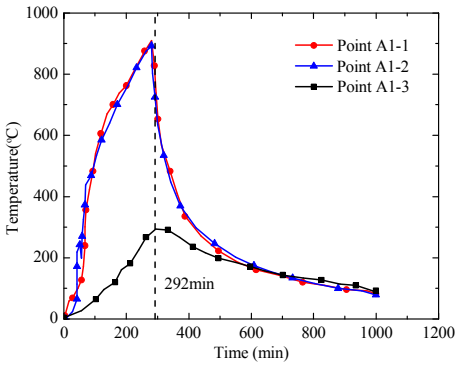

(g) Tree A1 (Test 4)

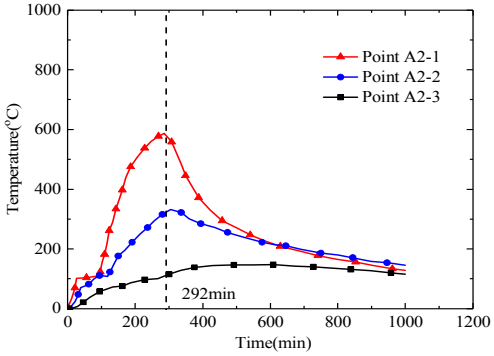

(h) Tree A2 (Test 4)

Fig. 15 Temperature versus time of the hollow slabs in Tests 1-4

Fig.16

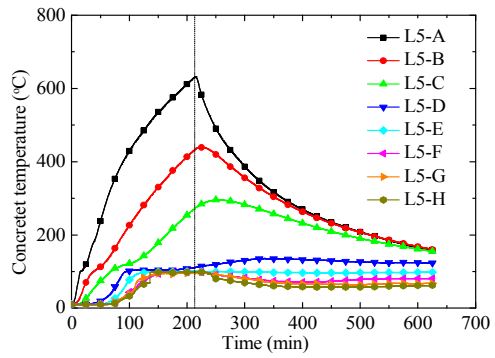

(a) L5 (Test 1)

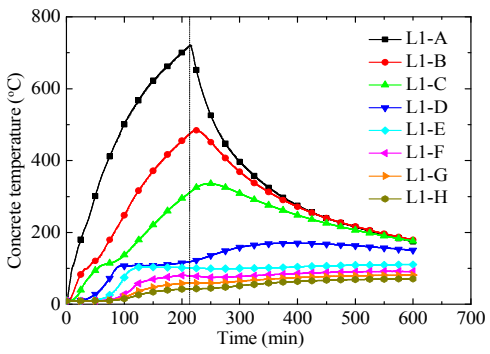

(b) L1 (Test 1)

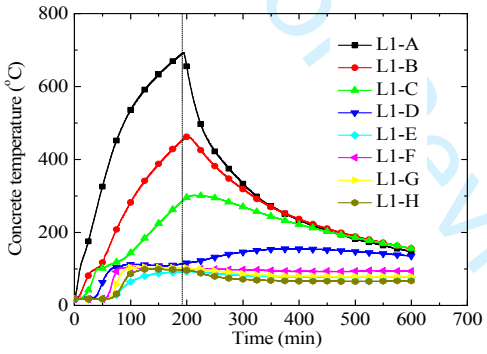

(c) L1 (Test 2)

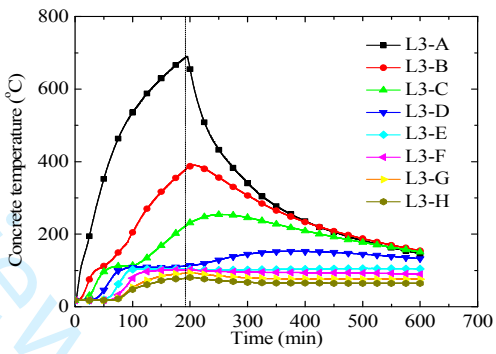

(d) L3 (Test 2)

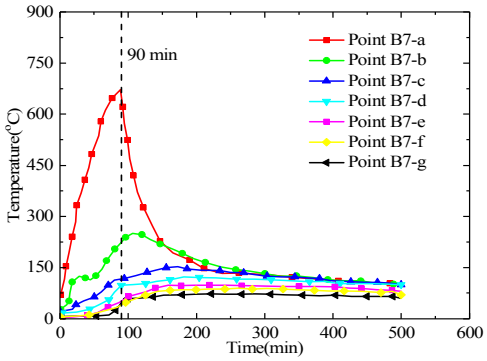

(e) Tree B2 (Test 3)

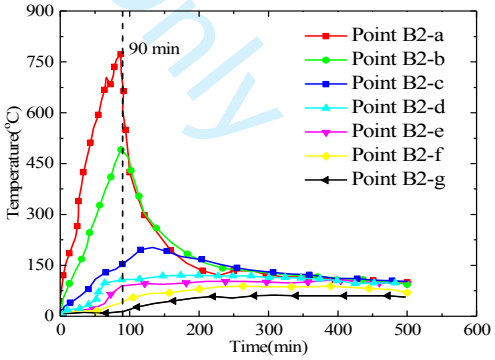

(f) Tree B7 (Test 3)

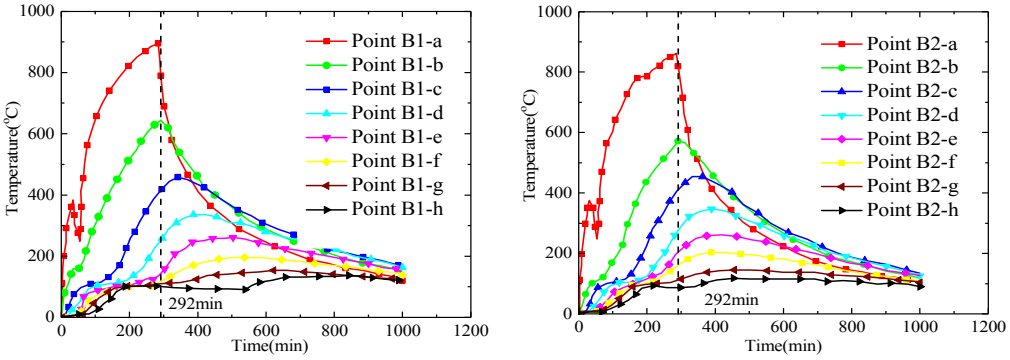

(g) Tree B1 (Test 4) (h) Tree B2 (Test 4)

Fig. 16 Temperature versus time of the ribbed beams in Tests 1-4

Fig.17

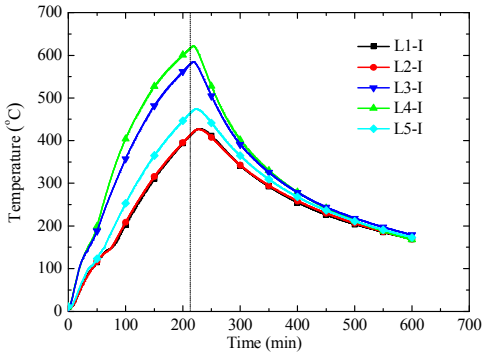

(a) Bottom steel bars (Test 1)

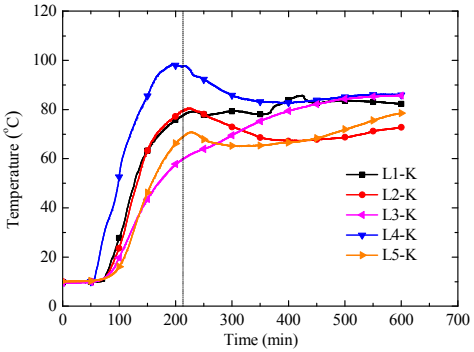

(b) Top steel bars (Test 1)

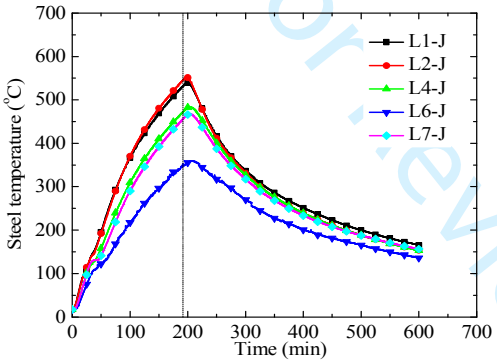

(c) Bottom steel bars (Test 2)

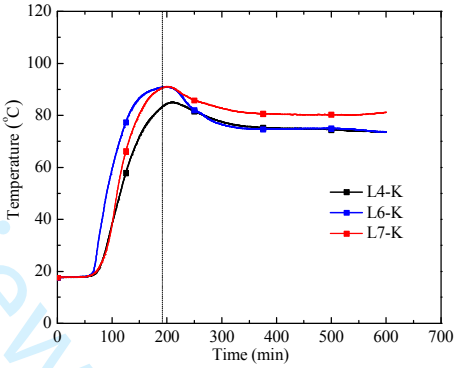

(d) Top steel bars (Test 2)

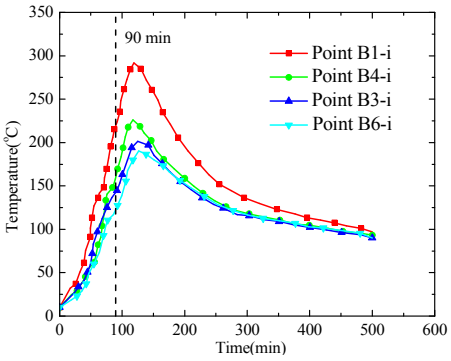

(e) Bottom reinforcing steels (Test 3)

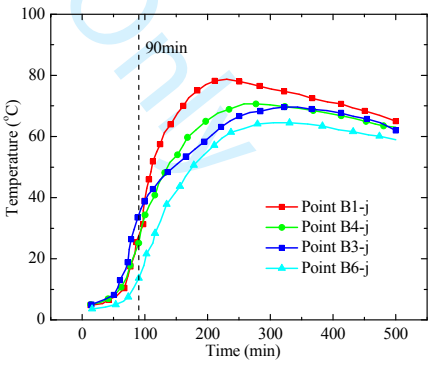

(f) Top reinforcing steels (Test 3)

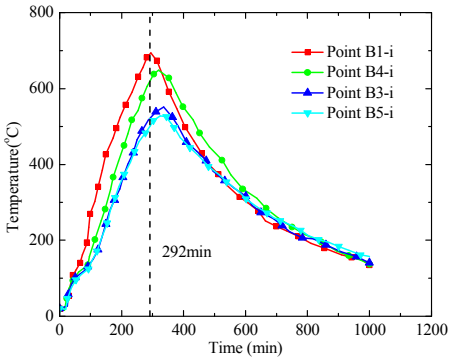

(g) Bottom reinforcing steels (Test 4)

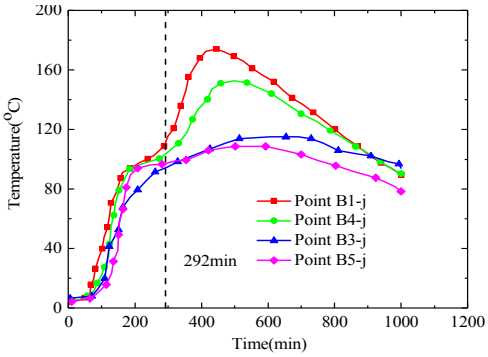

(h) Top reinforcing steels (Test 4)

Fig. 17 Temperature of the reinforcing bars in ribbed beams of four tests

Fig.18

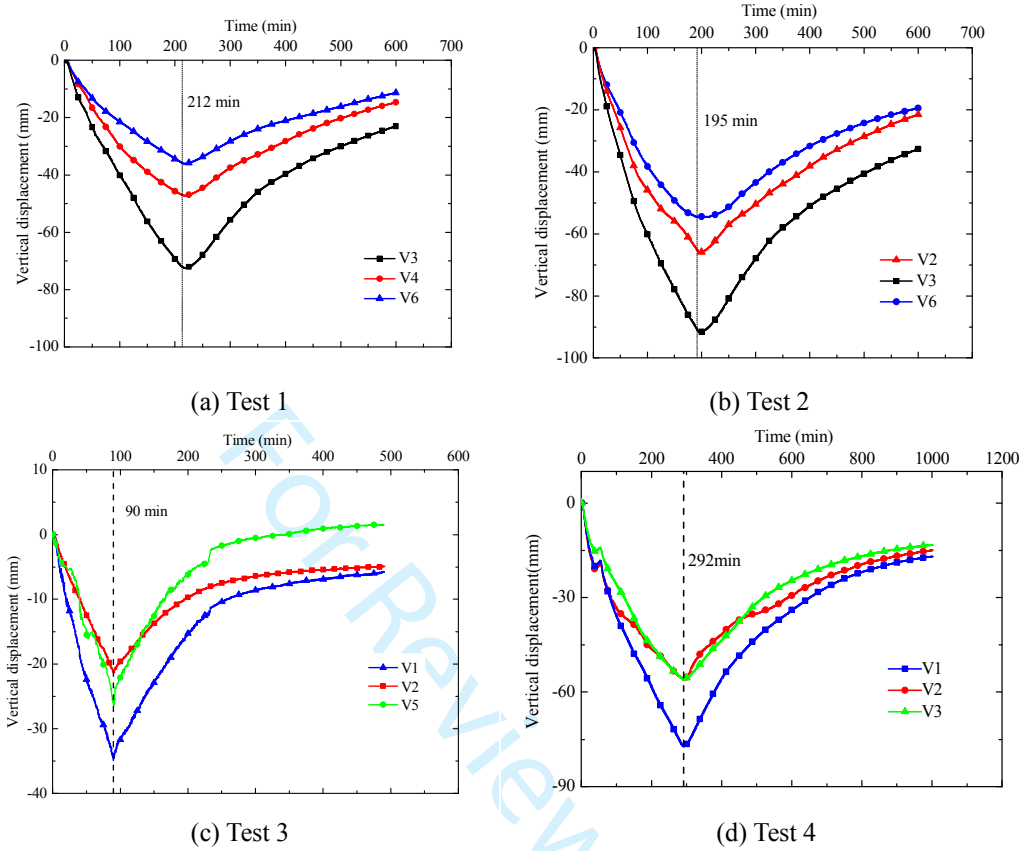

Fig. 18 Vertical displacement versus time in Tests 1-4

Fig.19

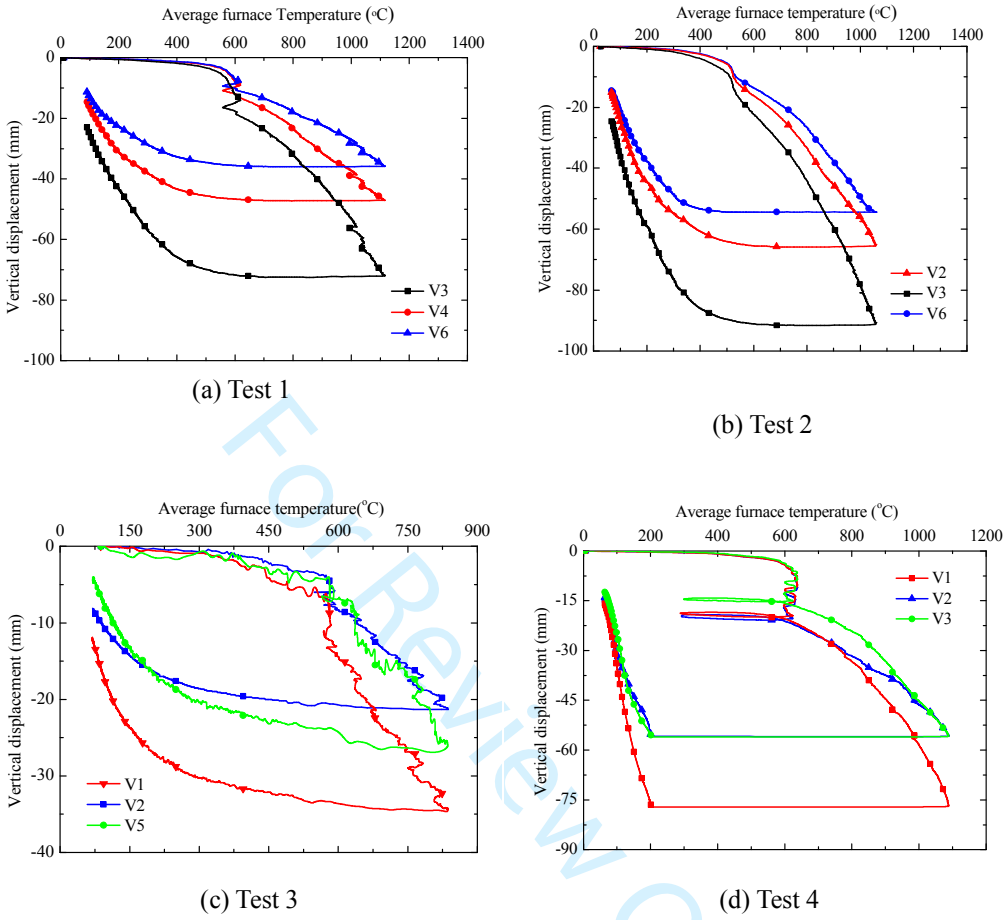

Fig. 19 Vertical displacement versus furnace temperature in Tests 1-4

Fig.20

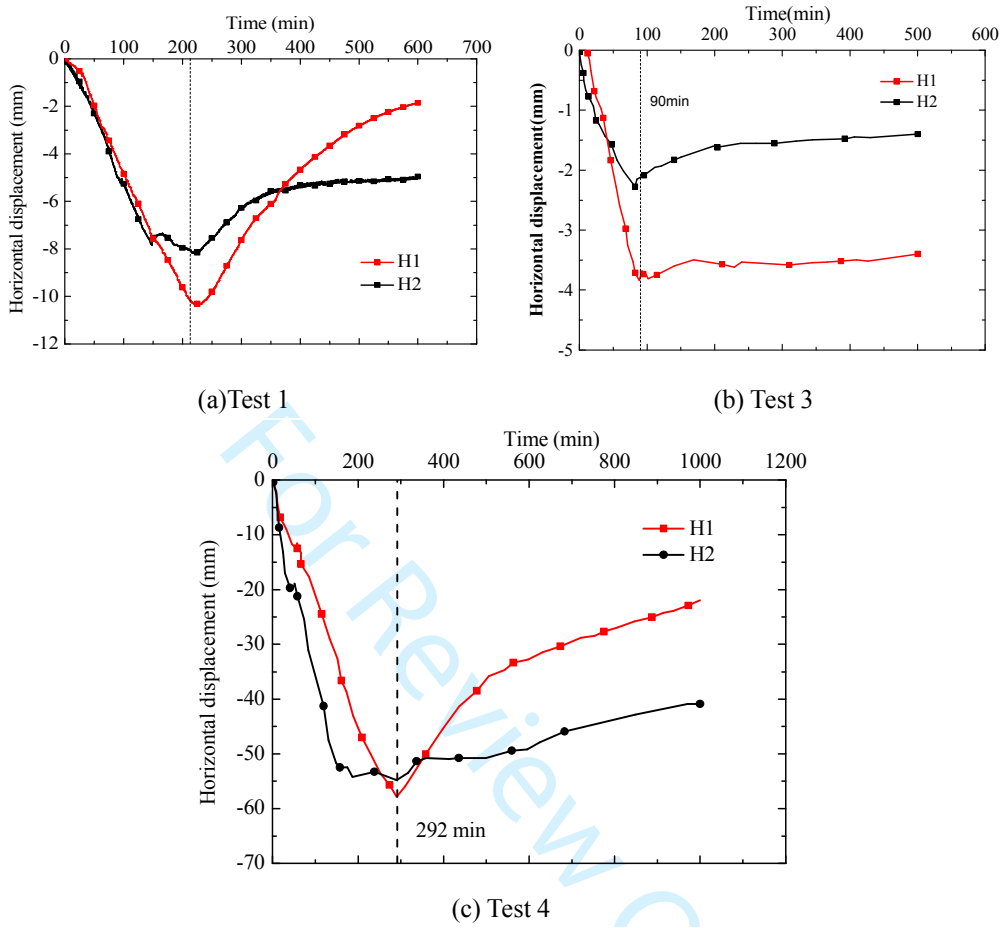

(a)Test 1 (b) Test 3

(c) Test 4

Fig. 20 Horizontal displacement versus time in Tests 1, 3 and 4

Responses to Reviewers' Comments

2 June 2018

Structural Concrete

Title of Paper: Experimental investigation on the fire resistance of cast-in-situ hollow core concrete slabs constructed using filler boxes and an assembly box system

Ms. Ref. No.: ID suco.201800060

Authors: Junli Lyu, Yong Wang, Ruben Van Coile, Zhaohui Huang, Yuner Huang

The authors wish to thank the reviewers for their valuable comments which certainly allow us to enhance the quality of this paper. The paper has now been revised after carefully considering referees' comments as follows:

Comment 1: "It is a good work but some details are missing. The number and units are separate to write. Please check it."

Response: This has been revised in the manuscript, modified places were marked in red.

Comment 2: "Give more details about the behavior of composite structure in fire. Please give the fire class of your slab."

Response: This has been clarified as:

See Page 7:

"2.6 Fire type

As discussed above, four fire tests were conducted on an oil-fired furnace, and the fire temperature followed the ISO 834 standard fire curve."

See Page 8:

"As shown in Figs. 11(e) and 11(f), full-depth cracks appeared at the edge beams in Tests 1 and 2. In addition, due to the mineral wool protection, little spalling occurred in the concrete columns (Test 2), as shown in Figs. 11(d), 11(g) and 11(h). However, as shown in Figs. 11(i) and 11(j), the concrete failure of two beam-column connections (i.e., south-east and north-east corners) occurred in Test 2 due

to the negative moment, and thus the connections in Test 2 should be reinforced to enhance their fire-resistant performance. ”

See Page 9:

“In addition, as shown in Fig. 12(e), the steel fracture in the assembly box occurred, and the spalling also appeared on the top plate. However, it is interesting to note that all the ribbed beams did not show the signs of serious spalling.”

See Page 10:

“Similar to that of Test 3, due to the serious spalling, a lot of concrete on the bottom surface had fallen off, and thus the steel bars exposed, as shown in Figs. 13(d) and 13(e). Hence, some methods should be used to reduce the risk of the explosive spalling in the unexposed or exposed assembly boxes. For example, the section shape or section size can be improved and the steel or polypropylene fibers added in the concrete mixes (Majorana et al., 2010).”

Figs. 11(e)-11(g), 12(e) and 13(e) were added in the revised manuscript.

“Majorana C. E., Salomoni V. A., Mazzucco G., Khoury G A.(2010). An approach for modelling concrete spalling in finite strains. *Mathematics and Computers in Simulation*, 80: 1694-1712.” was added in the revised mansucript.

Comment 3: *“*Page 2: Word Tade center is really a relevant exemplare for this manuscript?.*”*

Response: This has been clarified as (see page 2): “In recent years, a number of experimental studies have been conducted to investigate the fire behaviour of reinforced concrete slabs (Bailey and Toh, 2007; Li et al., 2015; Lim and Wade, 2002; Wang et al., 2016; Wang et al., 2018; Wang and Dong, 2009; Yang et al., 2013; Zhu, 2012), and it is acknowledged that reinforced concrete floor slabs play a key role in enhancing the fire resistance of the building. However, as noted in the following literature review, most of the tests considered conventional concrete slabs.”

Comment 4: *“*Page 2: Please give more information about the hollow core slabs. It depends on the structure, strength of the concrete.”

Response: This has been clarified as:

See Page 3:

"The slab consist of ribbed beams and 96 plastic boxes creating voids (each plastic box: 450 mm × 450 mm × 150 mm), as shown in Figs. 2(b)-2(f)."

See Page 4:

"Bottom and top reinforcing bars were arranged at a spacing of 200 mm along both directions, as indicated in Figs. 2(e) and 2(f)."

"In addition, the column construction, layout of plastic boxes and casting concrete are shown in Figs. 3(f)-3(h)."

See Page 5:

"Commercial fine aggregate concrete with the compressive strength of 40 MPa was used for the plate. Note that, the commercial fine aggregate concrete was designed according to the reference (JGJ 55-2011, 2011)."

"The photographs of top (bottom) plate, the side-wall, the assembly boxes and the reinforcing steels are shown in Figs. 4(i)-4(k)."

See Pages 5-6:

"The photograph of the assembly boxes and steels in Test 4 are shown in Fig. 5(e).

2.2.3 Concrete

The cast-in-situ concrete that was used in each test was the commercial concrete. The specified compressive strength of the concrete was 30MPa, and concrete mix was shown in Table 1. Slabs in Tests 1 and 2 were cast on the same day and were stored indoors in the laboratory to cure. The same procedure was followed for slabs 3 and 4.

The age of the concrete at the time of testing was: Slab Test 1=150 days; Slab Test 2 =120 days; Slab Test 3=60 days and Slab Test 4=120 days. Due to the testing conditions, the temperature and relative humidity were not controlled in the laboratory. The average compressive strength of the concrete was determined by three cubic crushing tests at the day of testing, with obtained strength values as discussed above."

Figs. 2(c), 2(d), 2(f), 3(f), 3(g), 3(h), 4(j), 4(k) and 5(e) were added in the revised manuscript.

Table 1 was added in the revised manuscript.

"JGJ 55-2011 Specification for mix proportion design of ordinary concrete (2011). Beijing: China Architecture & Buidling Press. (in Chinese)." was added in the revised manuscript.

Comment 5: "Page 3: There are missing important details, for example, concrete composition, and they influence the load-bearing capacity of the structure. Fig 12 and 13 you have spalling of concrete cover, that is influenced by the concrete composition. From the structure, they are too much information. Please select the relevant informations. The same is true for the diagrams!!!!"

Response: See the responses to Comments 2 and 4.